frontiers | Frontiers in Bioengineering and Biotechnology

TYPE Original Research
PUBLISHED 07 July 2023
DOI 10.3389/fbioe.2023.1211319

OPEN ACCESS

EDITED BY
Gloria Soberón-Chávez,
National Autonomous University of Mexico, Mexico

REVIEWED BY
Thorsten Heidelberg,
University of Malaya, Malaysia
Surekha K. Satpute,
Savitribai Phule Pune University, India

*CORRESPONDENCE
Agnieszka Lewińska,
agnieszka.lewinska@uwr.edu.pl
Marcin Łukaszewicz,
marcin.lukaszewicz@uwr.edu.pl

RECEIVED 24 April 2023
ACCEPTED 22 June 2023
PUBLISHED 07 July 2023

CITATION
Bochynek M, Lewińska A, Witwicki M, Dębczak A and Łukaszewicz M (2023), Formation and structural features of micelles formed by surfactin homologues.
Front. Bioeng. Biotechnol. 11:1211319.
doi: 10.3389/fbioe.2023.1211319

Formation and structural features of micelles formed by surfactin homologues

Michał Bochynek[1,2], Agnieszka Lewińska[3,4]*, Maciej Witwicki[3], Agnieszka Dębczak[5] and Marcin Łukaszewicz[1,2]*

[1]Department of Biotransformation, Faculty of Biotechnology, University of Wroclaw, Wroclaw, Poland, [2]InventionBio S.A., Bydgoszcz, Poland, [3]Faculty of Chemistry, University of Wroclaw, Wroclaw, Poland, [4]OnlyBio S.A., Bydgoszcz, Poland, [5]Łukasiewicz Research Network—New Chemical Syntheses Institute, Puławy, Poland

Surfactin, a group of cyclic lipopeptides produced by *Bacillus subtilis*, possesses surfactant properties and is a promising natural and biologically active compound. In this study, we present a comprehensive characterization of surfactin, including its production, chromatographic separation into pure homologues (C_{12}, C_{13}, C_{14}, C_{15}), and investigation of their physicochemical properties. We determined adsorption isotherms and interpreted them using the Gibbs adsorption equation, revealing that the C_{15} homologue exhibited the strongest surface tension reduction (27.5 mN/m), while surface activity decreased with decreasing carbon chain length (32.2 mN/m for C_{12}). Critical micelle concentration (*CMC*) were also determined, showing a decrease in *CMC* values from 0.35 mM for C_{12} to 0.08 mM for C_{15}. We employed dynamic light scattering (DLS), transmission electron microscopy (TEM), and density functional theory (DFT) calculations to estimate the size of micellar aggregates, which increased with longer carbon chains, ranging from 4.7 nm for C_{12} to 5.7 nm for C_{15}. Furthermore, aggregation numbers were determined, revealing the number of molecules in a micelle. Contact angles and emulsification indexes (E_{24}) were measured to assess the functional properties of the homologues, showing that wettability increased with chain length up to C_{14}, which is intriguing as C_{14} is the most abundant homologue. Our findings highlight the relationship between the structure and properties of surfactin, providing valuable insights for understanding its biological significance and potential applications in various industries. Moreover, the methodology developed in this study can be readily applied to other cyclic lipopeptides, facilitating a better understanding of their structure-properties relationship.

KEYWORDS

surfactin, *Bacillus subtilis*, homologues, micelles, adsorption, aggregation number

1 Introduction

Microbially derived compounds which possess hydrophilic and hydrophobic moieties, and exhibit surface active properties, are commonly referred to as biosurfactants. Compared to chemically derived surfactants, biosurfactants are independent of mineral oil as a feedstock. They are readily biodegradable and can be produced at lower temperatures. Additionally, increasing environmental awareness causes research to be undertaken to produce biosurfactants from biodegradable by-products. Surfactin (SU), which is produced by *Bacillus subtilis*, is becoming one of the best-known biosurfactants. A

great deal of previous research into SU has focused on its antifungal, antibacterial, antiviral, and antitumor properties (Vollenbroich et al., 1997; Wen et al., 2011; Wu et al., 2017; Horng et al., 2019) which result from its interaction with biological membranes caused by amphiphilic structure (Seydlová and Svobodová, 2008). However, because of this amphiphilic structure, SU also has interesting aggregation properties and thus can be used as a drug carrier, as demonstrated by our research group (Lewińska et al., 2020; Lewińska et al., 2021; Lewińska et al. 2022). Furthermore, the SU built into the colloidal systems shows synergism; is not only an interfacial stabilizer but also exhibits the properties of an active substance, e.g., antioxidant properties (Lewińska et al., 2021). Many publications demonstrated that SU is a promising agent in the removal of environmental pollutants, for example, in wastewater treatment or oil spillage neutralization (Singh and Cameotra, 2013; Mnif et al., 2015; Ndlovu et al., 2016). Its emulsifier properties enhance the bioavailability of oil ingredients, such as saturated hydrocarbons or polycyclic aromatic hydrocarbons, which then can be degraded by bacterial enzymes (Morán, 2000; Bezza and Chirwa, 2015; Parthipan et al., 2017). Besides its biological activities, cosmetic and pharmaceutical use, SU is also a high utility value molecule.

SU is a collective term used for a group of cyclic lipopeptides (CLP) with a ring composed of seven amino acids that is closed with the β-hydroxy-fatty acid moiety (Jajor et al., 2016). Like all CLPs, SU is produced in nonribosomal peptide synthesis (NRPS) from L-amino acids, D-amino acids and fatty acids (Bruner et al., 2002). Because of the substrate variety, structural differences may occur. Surfactin varies in the branching and length of the hydrophobic fatty acid chain. Three isomers, that is *n*-, *iso*- and *anteiso*-, and the lengths of 11–18 carbon atoms have been reported, but only the C_{12}-C_{17} homologues have been isolated (Kowall et al., 1998; Bartal et al., 2018; Qin et al., 2023). The most common sequence of the peptide loop is ELLVDLL, in which the second, fourth and seventh residue can be replaced with other amino acids like V, L, I or A. Regardless of the amino acid sequence, their chirality is always preserved (LLDLLDL) (Kowall et al., 1998). In the amino acid ring, two carboxyl groups (E and D) are present, constituting the hydrophilic part of the molecule, while the fatty acid chain forms the hydrophobic tail, to which SU owes its surface activity (surface tension from 72 to 27 mN/m) (Seydlová and Svobodová, 2008).

This publication presents a comprehensive study on the high-yield separation of a surfactin (SU) mixture into individual homologues, with a focus on determining their precise structures and aggregation properties. A wide range of analytical techniques, including chromatography, interfacial tensiometry, dynamic light scattering, transmission electron microscopy, and density functional theory, were employed to thoroughly characterize the homologues. Additionally, the wetting properties and emulsification indexes of the homologue solutions were investigated to gain insights into their dispersing capabilities in water. The findings from this study provide a deeper understanding of the structures and properties of surfactin homologues, with potential applications in diverse fields such as materials science and drug delivery.

TABLE 1 Gradient time program for flash separation.

Time [h:min:s]	Phosphate buffer [%]	Acetonitrile [%]
0:00:00	30	70
0:07:00	30	70
0:17:00	38	62
0:20:00	38	62
0:25:00	40	60
1:30:00	40	60
2:10:00	42	58
2:10:00	42	58
2:25:00	55	45

2 Materials and methods

2.1 Materials

LC-MS gradient-grade methanol and acetonitrile were purchased from VWR. Reagent grade salts [NH_4NO_3, $MgSO_4$, Na_2SO_4, KCl, $Fe_2(SO_4)_3$, $CuSO_4$, $MnSO_4$], HCl, H_2SO_4, and solvents (ethanol, ethyl acetate were purchased from Chempur (Tarnowskie Góry, Poland). Fermentation medium ingredients (yeast extract, MOPS, L-Val, L-Leu, L-Glu) of reagent grade were purchased from BioShop. LC-MS grade HCOOH and phenylthioisocyanate were supplied from Merck. The water used was miliQ using the HLP104V Hydrolab reverse-osmosis system (Wiślina, Poland).

2.2 Surfactin production and purification

In order to obtain a mixture of surfactin homologues, the lab-scale bioreactor Labfors3 (Infors AG) was used. 1.6 L of Landy medium (Jajor et al., 2016) (glucose 60 g/L, MOPS 21 g/L, NH_4NO_3 2.3 g/L, $MgSO_4$ 0.5 g/L, yeast extract 1 g/L, KCl 0.5 g/L, $Fe_2(SO_4)_3$ 1.2 mg/L, $CuSO_4$ 1.6 mg/L, $MnSO_4$ 5.6 mg/L and amino acids L-Glu, L-Leu, L-Val each 1 g/L, initial pH 7.5) was inoculated with *B. subtilis* 87Y strain to OD_0 = 0.1. Submerged fermentation was carried out at 37°C with 3.2 L/min airflow and 750 rpm stirring. After 24 h the process was terminated and the fermented medium was centrifuged (17,000 G, 10 min) in order to remove bacteria cells. Then the pH of the supernatant was adjusted to 2 with 6 M $HCl_{(aq)}$ and left overnight at 4°C. Next day the precipitated SU was centrifuged (17,000 G, 10 min) and lyophilized. Dry solid residue was then suspended in ethyl acetate, filtered through a short silica plug and dried under N_2 flow. The obtained SU was used for flash chromatography separation.

2.3 Flash chromatography

The surfactin mixture was separated into pure homologues with the use of a reversed phase flash column (Biotage® Sfär C18 Duo

100 Å, 30 μm—120 g) attached to Gilson PLC 2050 (pump system equipped with auto-collector). The mobile phase flow rate was set to 50 mL/min and it was composed of 20 mM phosphate buffer (pH = 6.5) and acetonitrile. Gradient time program is given in Table 1. 3.2 g of surfactin mixture was dissolved in 5 mL of initial mobile phase (buffer - MeCN, 3:7, [*v*/*v*]) and injected with a syringe directly onto the column. Fractions were collected by auto-collector in 25 mL glass tubes with the detector's threshold set to 200 mAU at wavelength 210 nm. The collected fractions were analyzed with HPLC-UV and those with the same homologues were combined to obtain C_{12}, C_{13}, C_{14}, and C_{15} surfactin. These combined fractions were evaporated to dryness with a rotary evaporator. Then the solid residue was dissolved in 50 mL of AcOEt, dried with anhydrous Na_2SO_4, pushed through a small silica gel plug with ethyl acetate (in order to remove inorganic impurities), filtered with a 0.22 μm nylon syringe filter and dried. The colorless, transparent, glass-like solid was dissolved in 10 mL of EtOH, diluted with the same volume of water, frozen in −80°C and lyophilized to get a product in the form of white powder with more than 99% purity.

2.4 HPLC-UV analysis of fractions

The fractions collected during flash separation were analyzed with a HPLC-UV system composed of two ECOM ALPHA 10 PLUS solvent pumps and detector UV-VIS EXOM Sapphire 600. The device was equipped with a 20 μL injection loop, KINETEX® 5 μm EVO C18 (100 Å, 150 mm × 4.6 mm) column and controlled by computer with Lp-Chrom® (Lipopharm.pl) software. From every 4th glass tube, 200 μL of fraction was diluted fivefold in MeOH and injected for analysis. The mobile phase (consisting of 15% water with 0.1% (*v*/*v*) HCOOH and 85% MeCN with 0.1% (*v*/*v*) HCOOH) was pumped with 1 mL/min flow in isocratic mode. 8 min was enough to elute all SU homologues from the column. The fractions containing one pure homologue were combined while the multicomponent fractions were rejected.

2.5 LC-MS analysis of surfactin homologues

Analyses were performed on Shimadzu LCMS-8040 system equipped with an ESI ion source and triple quadrupole mass detector. As the stationary phase Cortex C18 column (sizes: 4.6 mm × 50 mm, 2.7 μm) was used. During the experiment, the column was heated to 40°C and samples were kept at 10°C. Mobile phases were MeCN with 0.1% (*v*/*v*) HCOOH and water with 0.1% (*v*/*v*) HCOOH. The separation method was 10 min long with 1 mL/min flow rate of mobile phase and injection volume equal to 4 μL. The starting eluent was mixture 1:1 of MeCN and water and during the separation, the acetonitrile content was increasing. For the homologues' purity assay the analyzed mass range was 990–1,100 m/z in positive ion mode. The ion source temperature was set to 600°C, cone voltage 25 V and capillary voltage 0.8 kV. The desolvation gas was nitrogen. For fragmentation experiments, the collision energies (with argon as the collision gas) were optimized for every homologue in order to obtain the best mass spectrum.

2.6 Hydrolysis of surfactin

10 mg of each SU homologue was placed in glass ampoule with 1 mL of 6 M $HCl_{(aq)}$, flushed with gaseous N_2 and capped by melting the glass. The hydrolysis was conducted for 24 h in 110°C. Then the hydrolysates were transferred to 10 mL glass tubes, diluted with 3 mL portions of distilled water and extracted thrice with 3 mL aliquots of diethyl ether. Organic extracts were combined and evaporated under N_2 stream to give samples containing *β*-hydroxy-fatty acids. Water layers were lyophilized in order to obtain white, solid residues for amino acids analysis.

2.7 GC-MS analysis of fatty acids

Extracted *β*-hydroxy-fatty acids were derivatized in order to obtain methyl esters (You et al., 2015). Each sample was combined with 1 mL of 10% H_2SO_4 in MeOH, vortexed and incubated for 6 h in 55°C. Then after cooling down esters were extracted with diethyl ether (3 mL × 3 mL), dried and dissolved in 1 mL of methanol to be analyzed on Shimadzu GC-MS system (Shimadzu GC-MS TQ 8040) equipped with Zebron ZB-5MSi capillary column (30 m × 0.32 mm × 0.25 μm) with helium as a carrier gas (flow rate set to 1 mL/min). The column temperature was initially held at 60°C for 3 min, then elevated to 260°C at a rate of 8°C/min and maintained for 10 min. The EI ion source temperature was set at 220°C with 70 eV of ionization energy. The injection was performed at 250°C with sample volume equal to 5 μL at split ratio 20:1. The results were compared with the NIST11 Database.

2.8 HPLC-UV analysis of fatty acids

Amino acids were derivatized with phenylisothiocyanate (PITC) in order to obtain UV-absorbing products separatable on C_{18} column (Gonzalez-Castro et al., 1997). 0.3 mg of each sample isolated after hydrolysis was placed in glass vial and dissolved with 50 μL of redrying mixture (methanol-water-triethylamine 2:1:1 [*v*/*v*]). Solvents were removed under vacuum pump (160–180 mbar) and solid residue was mixed with 30 μL of derivatizing agent (methanol-water-triethylamine-PITC 7:1:1:1 [*v*/*v*/*v*/*v*]). After vortexing reaction was left for 20 min at room temperature and then placed under vacuum (160–180 mbar) for 4 h in order to remove solvents and derivatization byproducts. Dried samples were suspended in 300 μL of injection mixture (0.1 M phosphate buffer pH = 7.5 with 5% acetonitrile). Suspension was vortexed, agitated in ultrasound bath and centrifuged at 9050 G for 4 min before injection (10 μL). Analyzes were performed on ArcAcquity HPLC-UV system (Waters) equipped with Waters Pico-Tag column (300 mm × 3.9 mm; 4 μm) held at constant temperature 30°C. Eluent A was an aqueous 0.14 M sodium acetate with addition of triethylamine (0.5 mL/L) and pH set to 6.2 with glacial acetic acid. Eluent B was acetonitrile-water (40:60 [*v*/*v*]). The mobile phase flow and gradient were taken from (Gonzalez-Castro et al., 1997). Measured results were compared to the standards: L-Glu (E), L-Asp (D), L-Val (V), L-Leu (L) and L-Ile (I). The UV detector was set to 254 nm which is wavelength in absorption band of PITC phenyl ring.

2.9 Gibbs isotherms measurement

The surface tension measurements were performed at 295 ± 0.1 K using a Krüss K12 microprocessor tensiometer (Krüss, Hamburg, Germany) equipped with a du Nouy Pt-Ir ring (resolution ±0.01 mN/m). The surface tension data were obtained as the arithmetic mean of the values received from two independent runs; the data were reproducible within ±0.2 mN/m. From the data, the values of adsorption properties were calculated.

2.10 DLS measurement

Measurements were conducted at 298 K, using a Zetaseizer Nano Series (Malvern Instruments) equipped with ALV5000 multi-τ autocorrelator and He-Ne laser (632.8 nm) as a light source. The detection angle was set to 173° and samples were placed in disposable folded capillary cells (DTS1070) produced by Malvern Instruments. Each SU homologue was prepared as a solution of concentration equal to 10 × *CMC*, filtered through a 0.22 µm nylon syringe filter, placed in the measurement cell and left overnight to equilibrate before measurement. Analyses were performed in three runs and one run consisted of at least 10 measurements, and the obtained data is expressed as an average quantity with standard deviation. Due to the low solubility of pure SU in water, all measurements were done in 0.05 M TRIS×HCl (pH = 8.5).

2.11 TEM imaging

The transmission electron microscopy (TEM) imaging was performed using a FEI Tecnai G2 XTWIN transmission electron microscope (FEI, Hillsboro, OR, United States. The samples were prepared by placing a small amount of diluted suspension on a Cu-Ni grid and stained with 2% uranyl acetate before shooting. The size distribution plots were fitted using a Gaussian curve approximation.

2.12 DFT calculations

Computational techniques based on density functional theory (DFT) have been an effective tool for studying various chemical, biochemical or environmental problems (Ćwieląg-Piasecka et al., 2017; Rodríguez-Blanco et al., 2020; Witwicki et al., 2020; Witwicki et al., 2021; Cao et al., 2022; DeepikaVerma et al., 2022; Gorb et al., 2022) In our work, DFT calculations were conducted with the ORCA 5 suite of programs (Neese, 2012; Neese et al., 2020; Neese, 2022). In all DFT calculations, the resolution of the identity approximation (Neese, 2003; Kossmann and Neese, 2009; Neese et al., 2009), the dispersion correction with the Becke-Johnson damping scheme (D3BJ) (Grimme et al., 2010; Grimme et al., 2011), the conductor-like polarizable continuum model (CPCM) (Barone and Cossi, 1998) to cover solvent (water) effects, and the def2 basis sets (Weigend and Ahlrichs, 2005) in combination with the appropriate auxiliary basis set (def2/J) (Weigend, 2006) were used. Initial structures for geometry optimizations were generated using the genetic algorithm with the initial population of 200 conformers as implemented in OpenBabel 2.4.0 (O'Boyle et al., 2011). The geometry optimizations were carried out using the gradient-corrected functional BP86 (Perdew, 1986; Becke, 1988), which provides accurate molecular structures (Neese et al., 2010; Witwicki, 2015), the basis set def2-SVP, the tight SCF convergence criteria (TightSCF) and the default scheme for numerical integration (DefGrid2). Each of the stationary points was fully characterized as a true minimum through a vibrational analysis. On these molecular structures, single-point calculations were conducted with the hybrid functional B3LYP (Lee et al., 1988; Becke, 1993; Stephens et al., 1994), the basis set def2-TZVP, tightened SCF convergence criteria (VeryTightSCF) and increased accuracy of numerical integration (DefGrid3).

Electron density from these single-point calculations was analyzed with the Multiwfn 3.8dev code (Lu and Chen, 2012a). The electrostatic potential (EP) was studied on the van der Waals (vdW) surface defined as an electron density equal to 0.001 au. Such an approach to EP has been demonstrated to reflect accurately the possible electrostatic interaction between a molecule and other molecules (Bader et al., 1987; Lu and Chen, 2012b; Liu et al., 2021). Quantitative molecular surface analysis was carried out using the improved Marching Tetrahedra algorithm (Liu et al., 2021). EP was evaluated by regrouping the expression in terms of primitive Gaussian orbitals with identical angular momentum types and nuclei centers (Zhang and Lu, 2021). Molecular polarity index (MPI) was calculated as described in the literature (Liu et al., 2021). Visualizations were done with a combination of Gabedit (Allouche, 2011) and POV-Ray (www.povray.org) software.

2.13 Emulsification index

Emulsification indexes were determined with a standard method (Cooper and Goldenberg, 1987), where 6 mL hydrophobic fraction was added to 4 mL of surfactant solution of 150 mg/L concentration. Experiments were carried out in glass tubes with dimensions of 15 mm (internal diameter), 100 mm (length) and glass thickness of 1 mm. The bottoms were rounded and tubes were screw capped. After mixing samples were vortexed for 2 min at maximum speed and left to equilibrate for 24 h. After 24 h, the heights of the layers were measured (oil, emulsion, water and overall). In order to calculate E_{24}, the height of the emulsion layer was divided by the overall sample's height and expressed in percent:

$$E_{24} = \frac{h_{emulsion}}{h_{overall}} * 100\% \quad (1)$$

2.14 Contact angle assay

All samples were analyzed with the use of two different surfaces, glass (hydrophilic) and plastic - polyethylene (hydrophobic). In the experiments, solutions with 0.11 mg/mL concentrations of pure homologues in 0.05 M TRIS×HCl buffer (pH = 8.5) were prepared and placed on the surface as one droplet. Contact angles were measured with Kruss DSA 100 in standard conditions (273 K, 1,013 hPa) for hanging droplets.

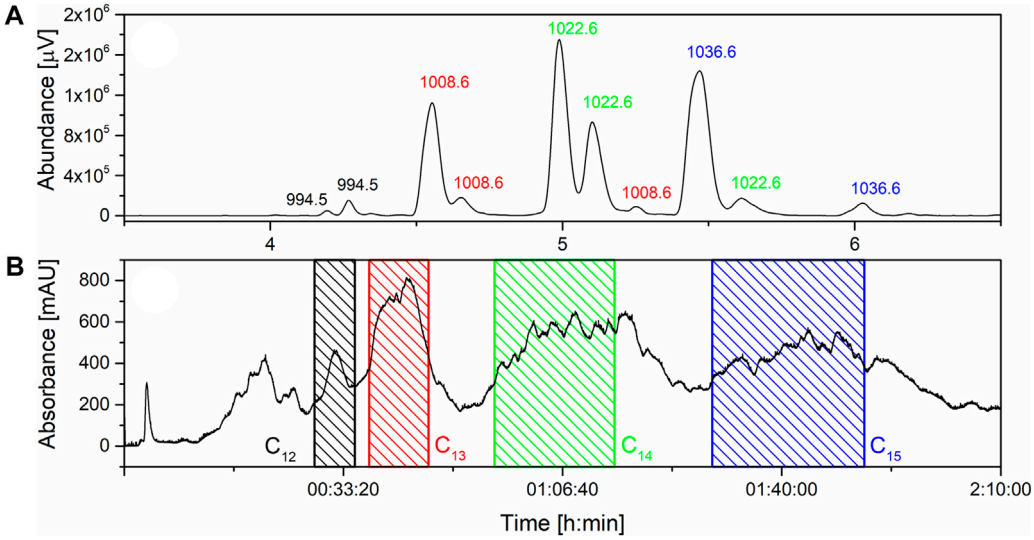

FIGURE 1
(A) composition of surfactin's mixture with m/z values; **(B)** Flash separation chromatogram with marked fraction collection.

3 Results and discussion

3.1 Flash chromatography

SU derived from microbial fermentation is a mixture of homologues (Figure 1A) which is typically purified via preparative-HPLC to obtain pure homologues with low yields (Peypoux et al., 1991; Kowall et al., 1998; Kracht et al., 1999; Kim et al., 2009). The first trials with flash chromatography involved a water-acetonitrile system as a mobile phase and C_{18} resin with particles sizes 100Å and 30 µM. However, due to the low solubility of pure SU in water dissolving even 1 g of analyte in 5 mL of initial mobile phase was impossible. For this reason, the water was replaced with a phosphate buffer with a concentration of 20 mM and pH stabilized at 6.5. This solution allowed to dissolve more than 3 g of SU in the injected volume (5 mL). First, the separations were tested in an isocratic mode with different mobile phase composition ratios. This approach turned out to be ineffective due to the very long separation time. Therefore, the method was modified and a gradient was introduced in which the concentration of acetonitrile increases with time starting from initial 30% (*v/v*). The gradient was optimized by multiple attempts to separate the SU into homologues shown in the chromatogram (Figure 1B). Using a column containing 120 g of C_{18} resin, it is possible to inject 3.2 g of SU in 5 mL of initial mobile phase and, as a result, isolate pure homologues C_{13}, C_{14} and C_{15} in amounts exceeding 100 mg. In addition, it is possible to isolate the C_{12} homologue, but in much smaller amounts due to its low content in the injected sample. Isolated fractions were analyzed with HPLC-UV apparatus in order to determine their compositions. All fractions containing pure homologues were combined and subjected to further isolation from mobile phase (described in materials and methods). Finally, homologues with over 99% purity were obtained. To our knowledge, this method is the most efficient way to isolate pure SU homologues enabling physiochemical and biological characterization (Peypoux et al., 1991; Kowall et al., 1998; Kracht et al., 1999; Kim et al., 2009).

3.2 Structural analysis of isolated homologues

SU compounds are a group of molecules that exhibit structural variability. First, they can form homologous series due to differences in the number of carbon atoms in *β*-hydroxy-fatty acid chains. Additionally, particular homologues can form isomers, as fatty acid moieties can exist in three branching patterns (*n*-, *iso*-, and *anteiso*-). Finally, analogues of surfactin can be distinguished based on differences in the amino acid substitution within the heptapeptide ring. Given the above facts, determining the exact structure of the particular SU homologue is not an easy challenge. Attempts similar to ours have been made in the past by, for example, (Grangemard et al., 1997) who characterized new variants of this compound. Their strategy was based on use of the NMR for *β*-hydroxy fatty acid branching determination, GC-MS in order to obtain information about its length and HPLC-UV for measurement of amino acids composition (Arutchelvi et al., 2009). have determined structures of homologues based on the HPLC-UV of amino acids and LC-MS measurement of molar masses but their strategy do not recognize the difference between homologue C_{12} with ELLLDLL and C_{13} ELLVDLL which have the same masses. To fully elucidate the structures of the isolated homologues, we initially assessed their purity using LC-MS in positive ion scanning mode, within the mass-to-charge ratio (m/z) range of 990–1,100 (Figure 2). In an electrospray ion source, surfactin gives adducts with protons $[M + H]^+$, sodium cations $[M + Na]^+$ and potassium cations $[M + K]^+$, so the expected m/z values of all homologues (listed in Table 2) are covered by the measured range (Tang et al., 2010; Bartal et al., 2018; Sun et al., 2019). The results proved high purity of the isolated surfactin homologues, shown by the pseudomolecular ions' masses. In the cases of C_{13} and C_{15}, single peaks were observed, but further analyses (GC-MS) have shown that their asymmetric shapes are caused by the overlapping of peaks indicating two different isomers. For C_{12} and C_{14}, mixtures of two isomers were measured–pair of peaks with the same m/z (994.5 for C_{12} and 1022.6 for C_{14}).

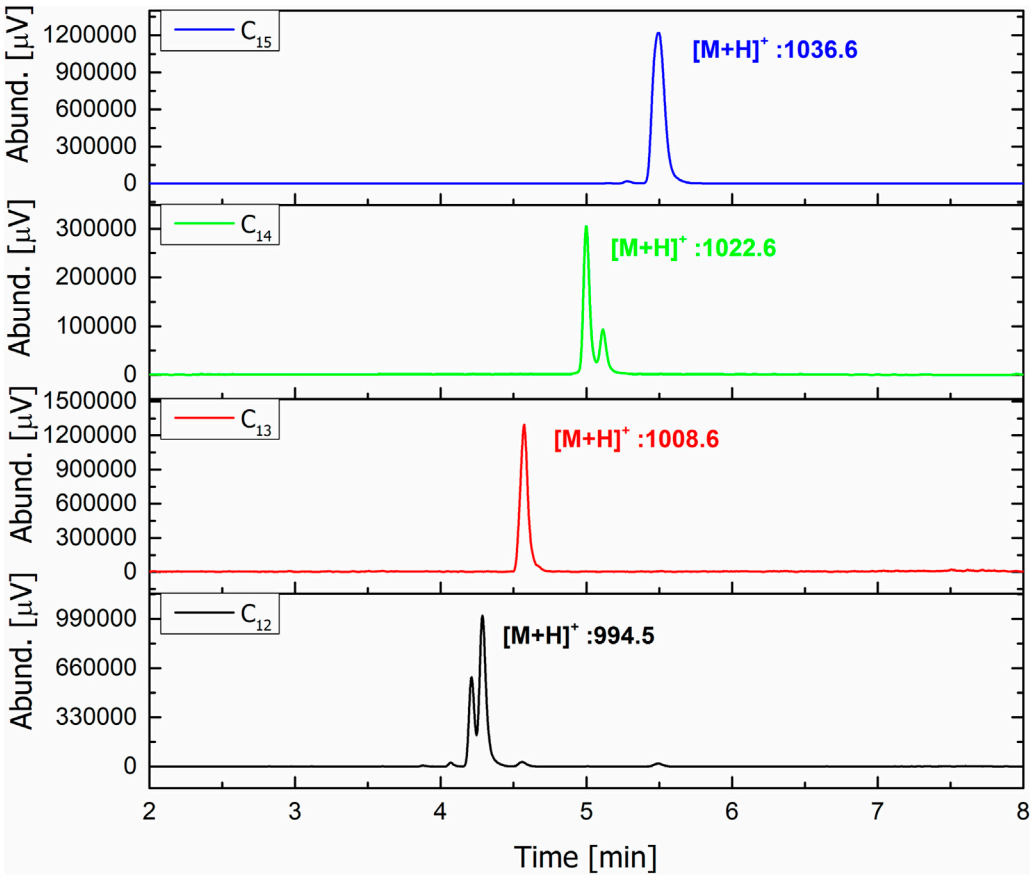

FIGURE 2
LC-MS scan mode chromatograms of purified fractions.

TABLE 2 Surfactin homologues molecular masses and m/z values of pseudomolecular ions.

Homologue	Molecular mass [Da]	m/z for $[M + H]^+$	m/z for $[M + Na]^+$	m/z for $[M + K]^+$
C_{12}	993.5	994.5	1,016.5	1,032.5
C_{13}	1,007.6	1,008.6	1,030.6	1,046.6
C_{14}	1,021.6	1,022.6	1,044.6	1,060.6
C_{15}	1,035.6	1,036.6	1,058.6	1,074.6

In most cases of surfactin production, the sequence of peptide ring is the same for all homologues produced in one batch, but there are some examples in literature showing that, for example, leucine (L) from 2nd position can be replaced with isoleucine (I), valine (V) from 4th position can be replaced with L or alanine (A), and L from 7th position can be replaced with I or V (Bartal et al., 2018; Hu et al., 2019). Therefore, to determine the amino acid sequences, MS/MS experiments were done. The first step was the selection of proper collision energies to obtain the best fragmentation patterns. It turned out that the longer the homologue, the higher the collision energy necessary, and finally −35 V was used for C_{12} and C_{13}, and -40 V for C_{14} and C_{15} homologues. In all cases, the following m/z fragmentation pattern was observed: 685.2 > 554.2 > 441.2 > 328.4. The m/z = 685.2 is the product of the ring opening and cleavage of the β-hydroxy-fatty acid and the glutamic acid (E), so the resulting ion is $[LLVDLL]^+$. Then, after the loss of the water molecule and N-terminal L, the $[LVDLL]^+$ ion is formed (m/z = 554.2). Removal of the C-terminal L gives the $[LLVDL]^+$ ion with m/z = 441.2. The last fragmentation reaction involves cleavage of the N-terminal L, resulting in the formation of an ion with m/z = 328.2 (Figure 3) (Ishigami et al., 1995; Tang et al., 2010). Such a fragmentation pattern was observed for all the analyzed homologues, indicating that the 4th position is V, and the 2nd position is either L or I, as mass spectrometry cannot distinguish

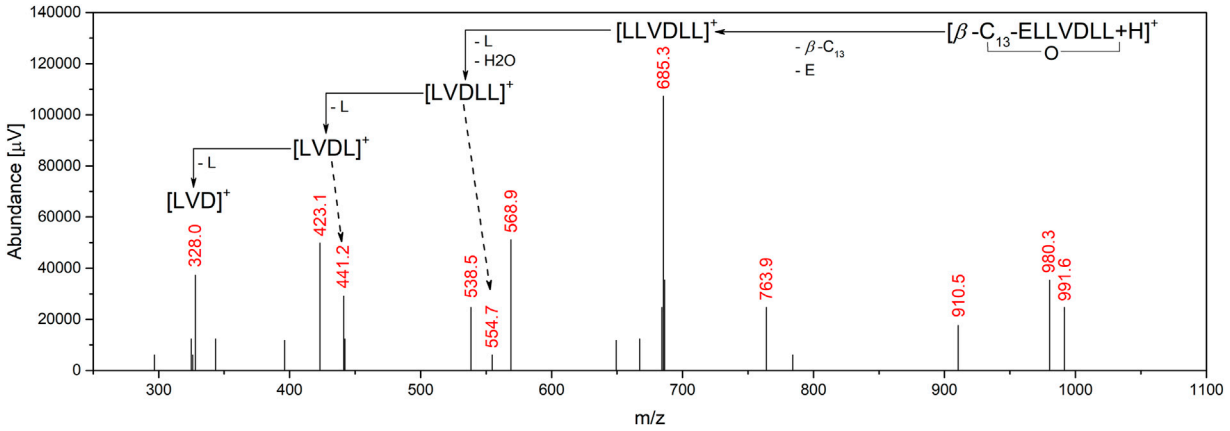

FIGURE 3
Fragmentation pattern observed on MS spectrum.

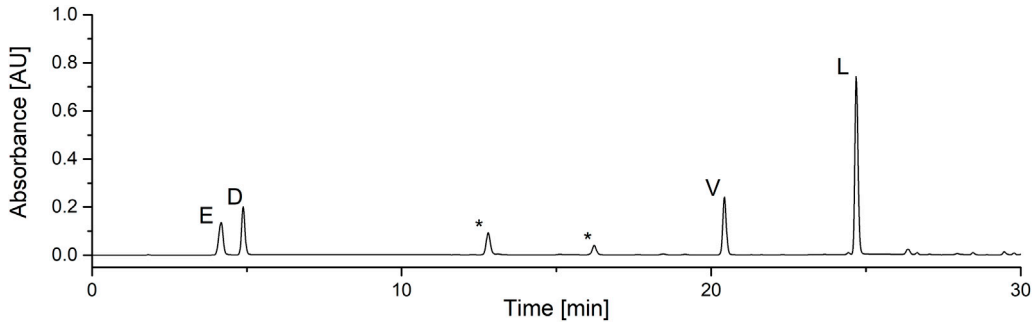

FIGURE 4
Example HPLC-UV analysis of PITC derivatized hydrolysates (measured for C15).

between these two amino acids. Therefore, amino acid content analysis using HPLC-UV was performed.

In order to exclude or prove I presence in the heptapeptide ring of SU's homologues, samples were hydrolyzed to amino acids and derivatized with the PITC (Bidlingmeyer et al., 1984). HPLC-UV results obtained for amino acid standards provided retention times: 4.20 min – aspartic acid (D), 4.88 min – glutamic acid (E), 20.42 min - valine (V), 24.33 min - isoleucine (I) and 24.70 min - leucine (L). These values compared with chromatograms measured for hydrolyzed homologues have shown an absence of I in all the homologues (chromatogram for C_{15} as an example shown in Figure 4). This means that all analyzed samples have sequence ELLVDLL, and the only structural differences between homologues are β-hydroxy-fatty acids. Between E and V peaks there are two non-identified peaks which are impurities (side products from derivatization of D and E, which were also observed in the standards' chromatograms). Integrals for E and D peaks are much lower than for V due to its weaker detector response factor, which is a known observation (Gonzalez-Castro et al., 1997). For V and L, the detector response factor is almost the same and the ratio between their peaks' areas is near 1:4, which is consistent with SU's ring sequence where there are 4 L and 1 V.

To elucidate entire homologues' structures, β-hydroxy-fatty acids' branching had to be determined. According to the literature, it can be stated that in cases of even numbers of carbon atoms in a homologue, the pair of *n-* and *iso-* isomers is produced. Odd numbered homologues form *iso-* and *anteiso-* pairs, which means that C_{12} has *n-* and *iso-* isomers, and C_{15} has *iso-* and *anteiso-* isomers (Kowall et al., 1998; Zhao et al., 2012) From the GC-MS with EI ion source measurement of fatty acids, pairs of isomers can be distinguished based on the value of I_{43}/I_{57} index (Figure 5). The *iso-* chain, as a direct product of fragmentation, forms a secondary carbocation $CH_3^+CH(CH_3)$, and in the case of the *n-* chain, the direct product is a primary carbocation $^+CH_2CH_2CH_3$, which then rearranges to the secondary one ($CH_3^+CH(CH_3)$). Thus, fragmentation to m/z = 43 for *iso-* chain is more preferable than for *n-*. For this reason, *iso*-branched fatty acid gives higher I_{43}/I_{57} than *n-*. The *anteiso-* chain gives a direct fragmentation product $CH_3CH_2^+CH(CH_3)$ with m/z = 57, so its I_{43}/I_{57} ratio will be lower than for *iso-*. It means that for the analyzed surfactin's

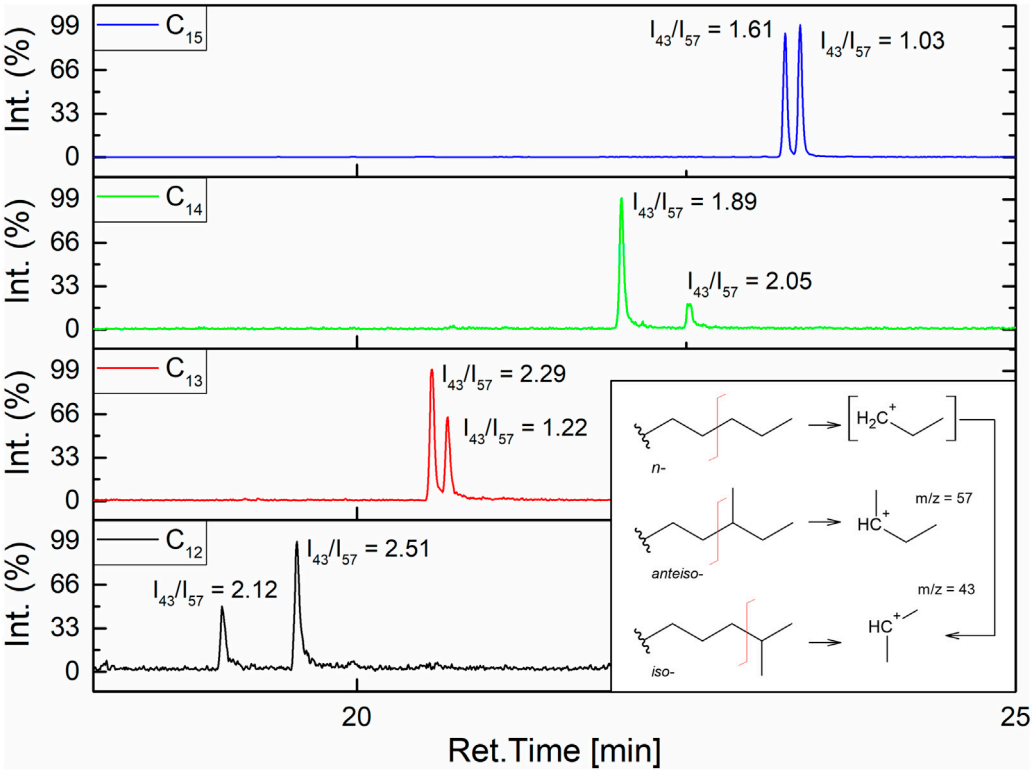

FIGURE 5
GC-MS analysis of β-hydroxy fatty acids in SU's homologues and calculated I_{34}/I_{57} indexes.

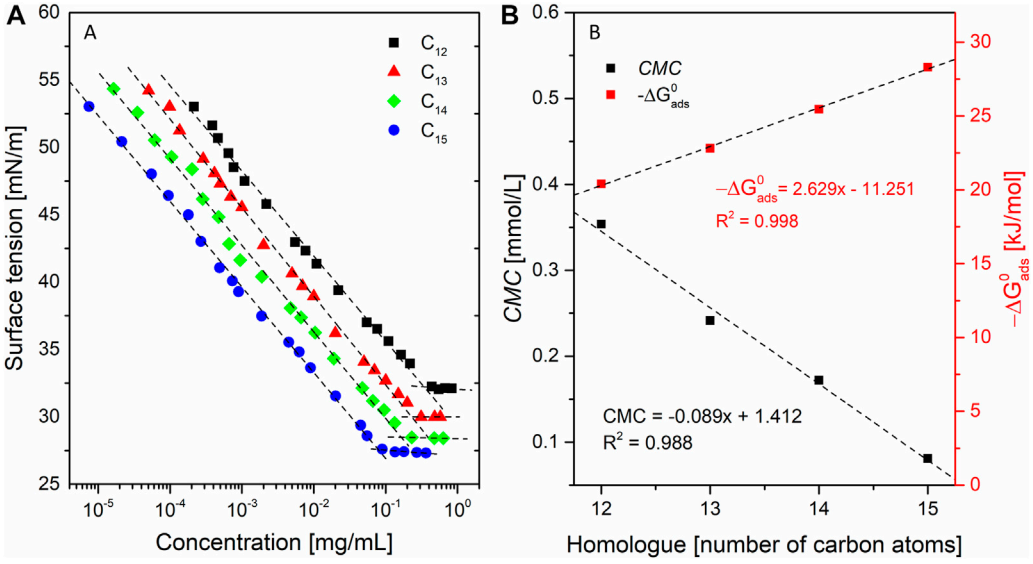

FIGURE 6
(A) equilibrium surface tension (γ) as a function of surfactant concentration; and **(B)** standard free energy of adsorption (ΔG^0_{ads}) a critical micelle concentration (CMC), of SU homologues as a function of the number of carbon atoms in the alkyl chain.

β-hydroxy-fatty acid isomers, this method can be used (Yang et al., 2007). The most stable fragmentation products are presented in Figure 5. GC-MS chromatograms (Figure 5) show two peaks for all homologues, which means that two different isomers are present in all the tested samples. I_{43}/I_{57} analysis for the obtained pairs shows that in the case of C_{12} and C_{14}, the first peak is a linear chain (*n*-),

and the second peak is *iso*-branched because the calculated index for *iso*- is higher than for *n*-. For C_{13} and C_{15}, there are *iso*- and *anteiso*-isomers, with the first peak on the GC-MS chromatogram corresponding to the *iso*-branched isomer. It was also observed that the retention times of *iso*- and *anteiso*- isomer pairs vary less compared to *n*- and *iso*- isomer pairs. As a result, the LC-MS chromatograms of *iso*- and *anteiso*- isomer pairs exhibit a single asymmetric peak, in contrast to the two separated peaks observed in the case of *n*- and *iso*- isomer pairs.

3.3 Gibbs isotherms measurement

The equilibrium surface tension isotherms for solutions of SU homologues in 0.05 M TRIS×HCl buffer (pH = 8.5) are shown in Figure 6A. The interfacial behavior of the SU homologues was studied through surface tension measurements performed at a wide range of surfactant concentrations. The surface tension isotherms and the adsorption parameters derived from the surface tension data were calculated. Classic interfacial behavior was observed as the surface tension decreases as the surfactant concentration increases. Once the minimum is reached, further addition of surfactant no longer changes the surface tension, so that the critical micelle concentration can be determined (Figure 6A).

The determined *CMC*s allow one to calculate the change of standard free energies of micellization (a measure of the tendency to form micelles), and reached 0.35, 0.24, 0.17, 0.08 mmol/L for C_{12}, C_{13}, C_{14}, and C_{15}, respectively. In any homologous series of surfactants, *CMC* regularly decreases with increasing hydrocarbon chain length and with increasing surfactant surface activity. This is because of Traube's rule, which says that in a homologous series of surfactants, each additional methylene group reduces the molar concentration required to reduce the surface tension of water by a factor of three. It means that for diluted solutions of surfactants belonging to one homologous series, in order to obtain the same reduction in the surface tension of the solution, three times lower molar concentration of the surfactant should be used compared to the compound containing one less methylene group in the hydrocarbon chain. It means that adding a methylene group reduces the *CMC* by a factor -log(1/3) = 2. However, deviations from this rule are possible, because it was formulated for simple compounds (such as aliphatic alcohols acids or esters) what should be noted during analysis of macromolecular compounds. Moreover, Traube's results were approximate since he used not sufficiently low concentrations to obtain linear part of the relation between concentration and surface tension. For the aliphatic alcohols and esters that factor was placed in the range of 2.7–3.2. It was also shown that for longer homologues that factor ranged from 1.2 to 5.8. Further research proved that Traube factor decreases for the compounds of high molecular weights (Traube, 1940). The development of that Traube's theory with more concentrated solutions gave factors in the wider range 2.5–4.1 (Ward, 1946). Taking into consideration abovementioned deviations it can be stated that our *CMC* values giving factors in pairs C_{12}-C_{14} and C_{13}-C_{15} equal to 2 and 3 agree with theory. Ignoring the differences in the shapes of the branching patterns obtained factors are: C_{12}-C_{13} (1.5) C_{13}-C_{14} (1.4), C_{14}-C_{15} (2.1). Figure 6B shows how the *CMC* value is influenced by the structure of the surfactant tail (its length)—the longer the alkyl chain, the lower the *CMC* value (Ueno et al., 1981). Determined *CMC* values agrees with the results of similar assays presented in literature (Arutchelvi et al., 2009). determined the *CMC* of crude surfactin isolated from YB7 strain of *B. subtilis* equal to 0.040 mmol/L in water basified with addition of NaOH. That value for mixture of homologues is lower than our determination for C_{15} but there is important difference in the buffering system. *CMC* values of surfactin measured in presence of Na^+ ions are significantly lower than in their absence (Li, Ye, et al., 2009). Also our not presented results have shown that in 0.01 PBS containing sodium salts *CMC* of C_{15} was measured to 0.020 mmol/L what is 4 times lower value than in 0.05 M TRIS×HCl (Zou et al., 2010). have measured *CMC* 0.015 mmol/L for C_{15} homologue in 0.01 M PBS what agrees our 0.020 mmol/L. Moreover the (Arutchelvi et al., 2009) do not specify the purity of isolated surfactin. The homologues are identified but their structures are not elucidated in exhaustive way. There is no clarity if compound described as C_{13} homologue is C_{13} with ELLDVLL peptide ring sequence of C_{12} with ELLDLLL. Nevertheless, the determined quantity is of the same order of magnitude. Similar results (*CMC* = 50 mmol/L) were published for surfactin standard purchased from Sigma and measured in PBS buffer (Shen et al., 2010). Another example is measurement of *CMC* for C_{16} homologue without the specified β-hydroxy fatty acid branching pattern (Li, Ye, et al., 2009). The experiment was conducted in the same buffer as in our assay and the author's result is 0.025 mmol/L. This is in accordance with Traube's rule and the tendency of the *CMC* to decrease with the elongation of the homolog molecule (Liu et al., 2008). presented *CMC* value 0.062 mmol/L for C_{12} homologue with the ELLVDLL sequence isolated with 90% purity. The measurement was conducted in 0.01 M PBS so the *CMC* was influenced by Na^+ ions. Moreover, the chromatogram presented in article suggests presence of longer homologues in the 10% of impurities which may have additionally diminish the *CMC*. The *CMC* for C_{17} homologue measured in 0.01 M PBS by (Qin et al., 2023) was 0.004 mmol/L which also agrees with the Traube rule and the tendency to lower the micellization concentration with addition of following methylene groups and presence of Na^+ ions. The presence of branches in the chain has an impact on ΔG^0_{ads}, causing its decrease due to the steric hindrance to aggregate in bulk (Varadaraj et al., 1992). The surface activities, measured as ΔG^0_{ads}, were obtained from the equation:

$$\Delta G^0_{ads} = -0.45\,nC + 5.17 \tag{2}$$

Surface activity's increase with the length of the alkyl chain was observed and its dependence on the number of carbon atoms in the alkyl chain for SU appears to be linear (Figure 6A):

The obtained surface tension data were used to calculate the characteristic adsorption parameters from the Gibbs adsorption equation:

$$\Gamma_\infty = -\frac{1}{nRT}\frac{d\gamma}{dln_c} \tag{3}$$

where Γ [mol/m^2] is the surfactant surface excess concentration, γ [mN/m] is the surface tension, c [M] is the surfactant concentration,

TABLE 3 Adsorption parameters of surfactin homologues.

Homologues	γ_{min} [mN/m]	$10^6\ \Gamma_\infty$ [mol/m^2]	$10^{20}\ A_{min}$ [Å^2]	pC_{20} [M]	$-\Delta G^0_{ads}$ [kJ/mol]	*CMC* [mmol/L]
C_{12}	32.2	2.57	149	$2.43*10^{-4}$	20.41	0.35
C_{13}	30.0	2.60	147	$9.13*10^{-5}$	22.81	0.24
C_{14}	28.5	2.50	153	$3.11*10^{-5}$	25.43	0.17
C_{15}	27.6	2.45	156	$9.79*10^{-6}$	28.29	0.08

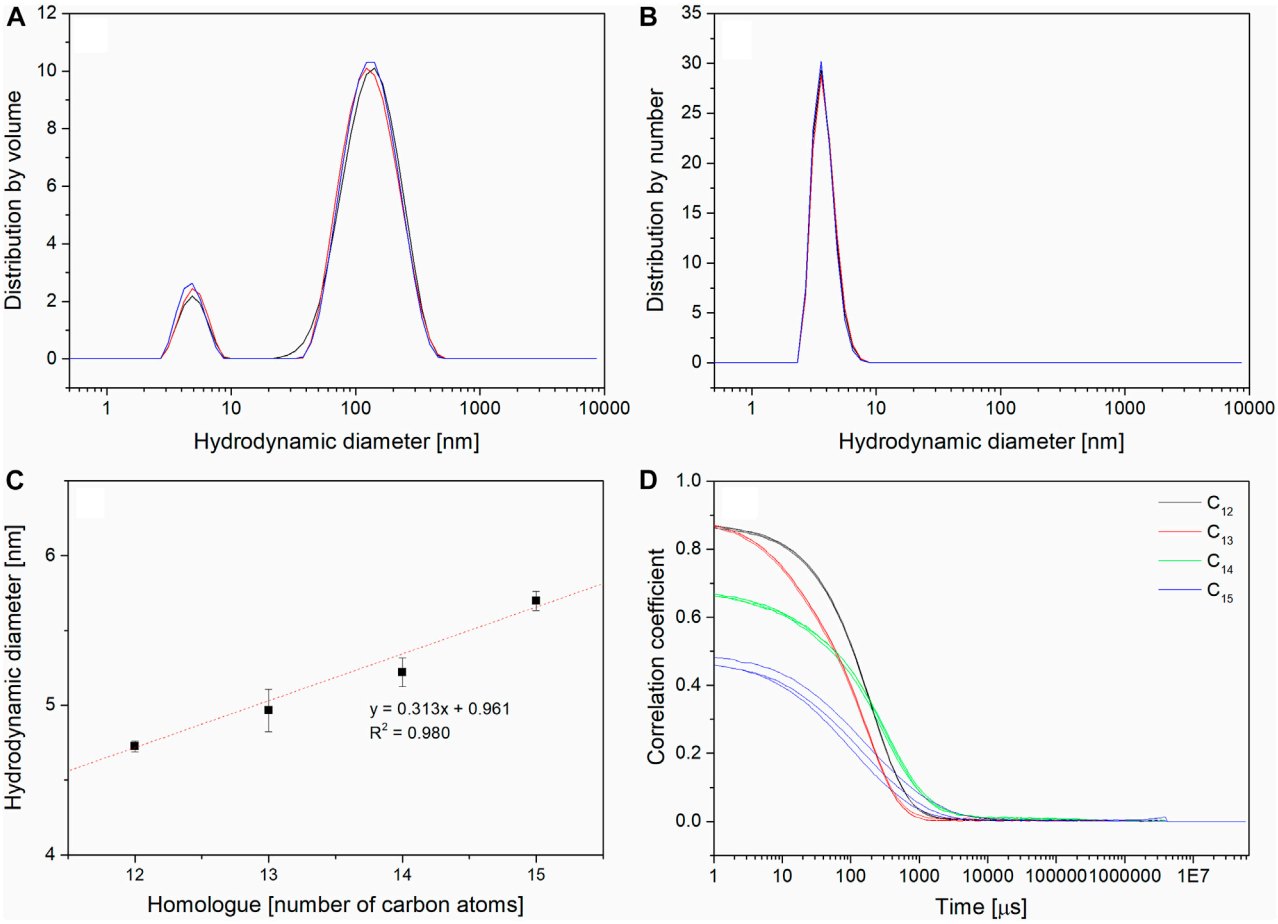

FIGURE 7
DLS results: **(A)** size distribution in terms of volume for C13 (3 replicates); **(B)** size distribution in terms of number for C13 (3 replicates); **(C)** comparison of homologues' hydrodynamic diameters; **(D)** comparison of homologues' correlograms (overlay of 3 measurements for every homologue).

R [J/(mol K)] is the gas constant and T [K] is the absolute temperature. The minimum surface area demand per molecule, A_{min}, was calculated from the equation:

$$A_{min} = \frac{1}{N_a \Gamma_\infty} \tag{4}$$

where N_A is the Avogadro number. The values of the obtained parameters for the investigated surfactants are shown in Table 3. Our results of A_{min} agrees with literature. (Shen et al., 2009) have determined experimentally 147 Å^2 with SANS and compared it to the Gibbs equation results obtained in non specified buffer system (132 Å^2) by (Maget-Dana and Ptak, 1995). The values shown increasing tendency with elongation of homologue chain within C_{12},C_{14} and C_{15}. The difference between C_{12} and C_{13} is negligible.

$$\Delta G^0_{ads} = -2,303\ RT\ pC_{20} \tag{5}$$

where pC_{20} is surface adsorption efficiency as the negative logarithm of bulk surfactant concentration C_{20} required to reduce the surface tension of water by 20 mN/m. The more negative the ΔG^0_{ads} values, the greater the tendency for the surfactant to adsorb at the air/water interface. Thus, the values of ΔG^0_{ads} in Table 1 show that an increased length of hydrocarbon chain promotes greater adsorption activity.

TABLE 4 Properties of examined micellar systems predicted at the DFT theory level: molecular polarity indexes (MPI), minimal (EP_{min}) and maximal (EP_{max}) values of electrostatic potential, micelle diameters (d_{mic}), molecular volumes of monomeric SU (V_{mon}), micelle.

		MPI [kcal/mol]	EP_{max} [kcal/mol]	EP_{min} [kcal/mol]	d_{mic} [nm]	V_{mon} [nm^3]	V_{mic} [nm^3]	N_{agg}
C_{12}	*anteiso-*	78.2	1.85	−182.39	3.84	1.33	29.89	22
	iso-	77.9	1.85	−182.35	3.86	1.34	30.26	23
	n-	77.5	1.82	−182.32	4.12	1.34	36.61	27
	exp from DLS	—	—	—	4.7	—	—	—
C_{13}	*anteiso-*	77.0	1.78	−182.29	4.12	1.36	36.45	27
	iso-	76.9	1.71	−182.24	4.14	1.36	37.29	27
	n-	76.6	1.82	−182.33	4.34	1.36	42.68	31
	exp from DLS	—	—	—	5.0	—	—	—
C_{14}	*anteiso-*	76.1	1.82	−182.27	4.36	1.38	43.57	31
	iso-	76.0	1.89	−182.28	4.32	1.38	42.41	31
	n-	75.7	1.78	−182.31	4.60	1.39	50.87	37
	exp from DLS	—	—	—	5.2	—	—	—
C_{15}	*anteiso-*	75.2	1.64	−182.24	4.62	1.41	51.87	37
	iso-	75.0	1.67	−182.26	4.62	1.41	51.33	36
	n-	74.8	1.80	−182.33	4.82	1.41	58.74	42
	exp from DLS	—	—	—	5.7	—	—	—

3.4 DLS measurement

Pure surfactin in form of protonated acids is insoluble in water, so DLS measurements were conducted in 0.05 TRIS×HCl buffer (pH = 8.5) which is typically used to observe single micelles without aggregates (Li, Zou, et al., 2009; Jauregi et al., 2013). Homologues were analyzed in order to determine hydrodynamic diameters of formed micelles. Size distributions by relative intensities and relative number were compared. In the case of all four homologues, the relative intensity distribution shows two populations, a weak peak for sizes 4–6 nm (single micelles) and a three times higher peak for aggregates with over 100 nm (shown on Figures 7A, B with C_{13} as an example). Recorded signal is much stronger for big aggregates than for small ones. The light scattering strongly depends on the volume of particles: the big ones give a strong signal even in small amounts because the radius cubed gives the volume (Abe, 2019) So compared to the distribution by number (where only single micelles are observed), it can be stated that single micelles are the major population of the sample (Han et al., 2008). The measured sizes ranged from 4.7 nm (for C_{12}) to 5.7 nm (for C_{15}) (Table 4 *exp. DLS*). Similar sizes were reported for SU mixture by other authors (Han et al., 2008; Zou et al., 2010; Jauregi et al., 2013) but there is no available data about pure homologues micellar sizes set together. Comparison of results regarding the homologue chain length showed a linear dependence, where the diameter of the micelles increases with the increase of the number of carbon atoms (Figure 7C). Such observation was expected based on other research done on homologues of surfactants (Gracia et al., 2004; Lewińska et al., 2014). From C_{12} to C_{15}, the micelles become less spherical and more oval, which is confirmed by measured correlograms (three for every homologue) showing a decrease in correlation coefficient (CC) with an increase of carbon atom number in the homologue (Figure 7D). So far, the published data on SU mixture micelles provides observation of cylindrical shapes in pH 9.5 which moved to the spherical and ellipsoidal ones after NaCl and $CaCl_2$ addition (Knoblich et al., 1995). It shows that the shape of SU's aggregate is environment-dependent. The presence of complexing cations can promote formation of higher order aggregates. It could explain why in the PBS and $NaHCO_3$ large (about 100 nm) aggregates are measured instead of single micelles (Li, Zou, et al., 2009; Liu et al., 2015). Such big aggregates were also observed in other assays as, for example, (Arutchelvi et al., 2014) where the sizes distribution for mixture of surfactins was investigated. Populations of 180 nm and 800 nm sizes were observed and explained with formation of vesicles and large aggregates (Zou et al., 2010). also shows the presence of aggregates different than single micelles described as large fractal ones based on the small angle neutron scattering and freeze-fracture transmission electron microscopy data. Their presence is explained by the hydrogen bonds formation between peptide rings of surfactin.

In order to prove the decrease in spherical shape of single micelles, the correlograms were compared. The value of correlation coefficient in DLS measurement provides information about the quality of the measured data. The lower its value in t_0, the lower the correlation of measured scattered light (Goldburg, 1999). An ideal and practically unattainable situation is CC equal 1, but in reality, every measurement with CC above 0.8 is adopted as high-quality data. In homologous series, it can be observed that for C_{12} and C_{13} CC values are good, but for C_{14} the CC value decreases, and for C_{15} it reaches the lowest level. Additionally, for C_{12}, C_{13} and C_{14},

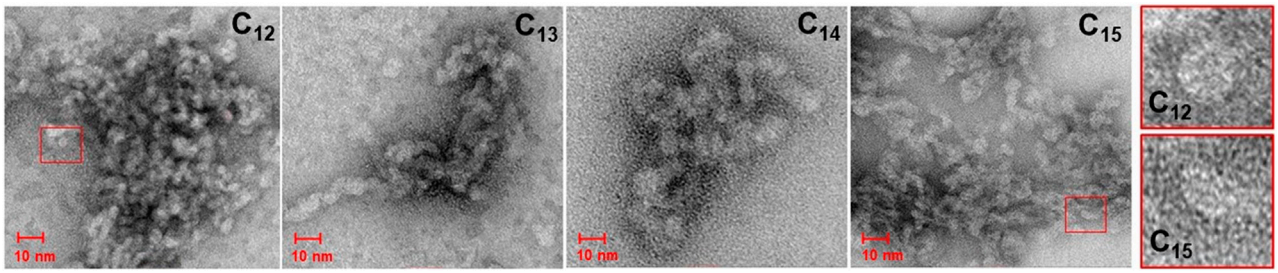

FIGURE 8
TEM imaging of surfactin homologues micelles and shape comparison.

all three replicates of correlograms are identical, while for C_{15} they vary, which suggests variations in measurements resulting most probably from the change in shape. DLS is a method dedicated for spherical nanoparticles, so every difference in shape causes higher variation of measurement (Pecora, 2000; Stetefeld et al., 2016). Moreover, irregular shapes can cause overestimation of the hydrodynamic diameters due to the stronger light scattering of the bigger dimension. This effect can be additionally enhanced by the hydration shell (Varga et al., 2020). The observation of sphericity disturbance with increasing length of the homologue was supported by TEM observations and the results of DFT calculations.

3.5 TEM

Transmission electron microscopy was used to investigate the morphology of the obtained micelles (Figure 8). TEM imaging revealed quasi-spherical shapes. A subtle change of shape from spherical to eliptic with increasing length of hydrophobic chain was observed. The observed sizes, after considering the contrast layer, were in reasonable agreement with the DLS measurements. Some differences could have resulted from the different sample preparation processes and different measurement techniques.

The change of spherical to more cylindrical shape of micelles formed by SU homologues with growing hydrophobic tail from C_{12} to C_{15} is most probably due to a combination of three factors: increased hydrophobic interaction between the tails, decrease in *CMC*, and decreased curvature of the micelle surface (formation of lager micelles). The spherical shape of micelles formed by surfactants is a delicate balance between the hydrophobic and hydrophilic properties of the surfactant molecules. As the hydrophobic tail of a surfactant molecule grows from C_{12} to C_{15}, the hydrophobic interaction between the tails becomes stronger. In a spherical micelle, the hydrophobic tails are arranged radially around the center of the micelle, with the hydrophilic head groups facing outward. This arrangement maximizes the surface area of the hydrophobic tails that can be shielded from the aqueous environment, while minimizing the surface area of the hydrophilic head groups that are exposed to water. As the hydrophobic tail grows longer, they occupy bigger volumes leading to increased hydrophobic interaction between the tails, which can cause the surfactant molecules to pack more tightly, reducing overall or local curvature of the micelle surface (changing shape and diameter, which has grown from 4.7 to 5.7 nm). Additionally, the increase in the size of the hydrophobic tail leads to a decrease in the critical micelle concentration *CMC* (from 0.35 to 0.08 M). As the *CMC* decreases, the concentration of surfactant molecules in solution increases, contributing to the formation of larger micelles, which may have a more cylindrical shape.

3.6 DFT computations

We performed all the DFT computations for the anionic form of SU (deprotonated carboxyl groups of Glu and Asp) because the DLS experiments were performed in TRIS×HCl buffer (pH = 8.5).

All the SU homologues are highly asymmetric systems and have non-zero dipole moment. To illustrate the polarity of SU, we calculated molecular polarity index (MPI), which is a descriptor expressed as (Liu et al., 2021):

$$MPI = \frac{1}{A}\iint_S V(r)|dS \tag{6}$$

where A and V(r) refer to the area of van der Waals (vdW) surface and the value of EP at a point **r** in space, respectively. In eq. X6, the integration is performed over the whole molecular vdW surface (S). The calculated MPI values of the SU homologues are listed in Table 4 and are found to be in the range 74.8–78.2 kcal/mol. The MPI value decreases with the *β*-hydroxy fatty acid length and is always slightly lower for *anteiso-* and *iso-* than for *n-* isomer. The polarity of SU is high since the predicted MPI values are significantly higher in comparison with the corresponding indexes reported previously for model nonpolar systems, that is 2.6, 6.7, and 8.4 kcal/mol for ethane, ethene, and benzene, respectively (Liu et al., 2021). They evince that the electrostatic interaction between SU and other polar molecules should be fairly strong. However, local polarity in the SU molecules should vary because all heteroatoms are distributed only in the peptide ring. An electrostatic potential (EP) map should be an efficient tool for illustrating the local SU polarity.

The isosurface maps of the EP for three isomers of C_{12} are shown in Figure 9. From these isosurfaces, it can be seen that most regions of SU show negative EP, as expected for an anionic molecule, in contrast to polar neutral molecules for which clear positive and

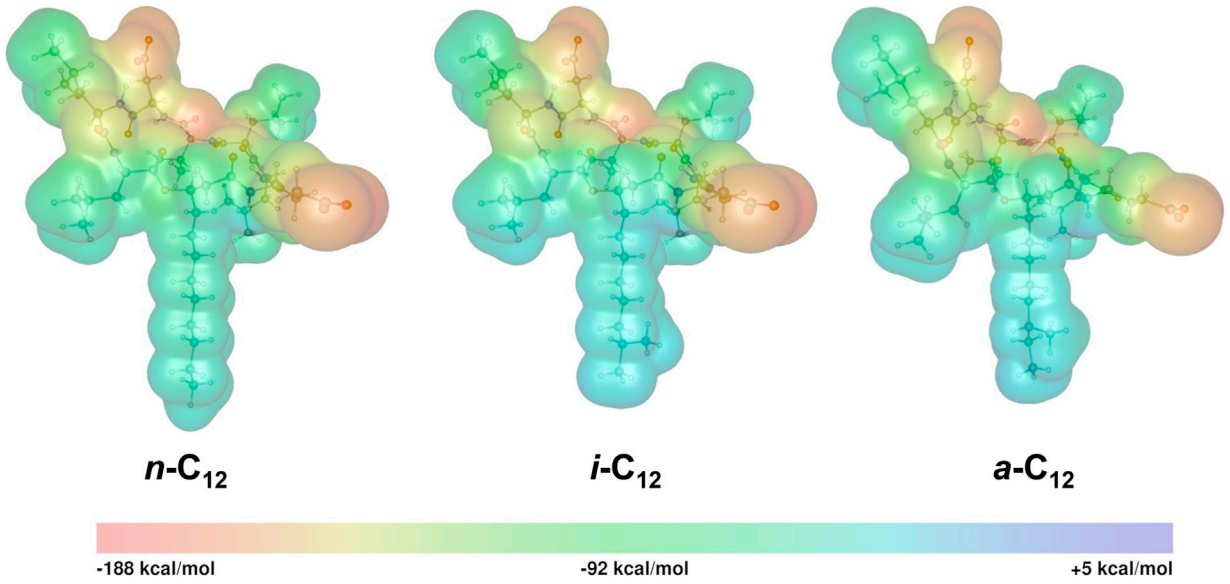

FIGURE 9
Isosurface maps of the EP for three isomers of C_{12} homologue (isovalue 0.001 au) calculated with the functional B3LYP and basis set def2-TZVP.

negative zones are expected (Lewińska et al., 2021). Although the EP is generally negative, its distribution is strongly irregular, with the minimal (EP_{min}) and maximal (EP_{max}) values of ca. −182 and +2 kcal/mol, respectively. The EP_{min} and EP_{max} values are given in Table 4.

In SU, the most negative regions are circular and surround oxygen atoms in the peptide ring. As discussed by Durán-Álvarez et al. (Durán-Álvarez et al., 2016), such a strong charge localization reflects a hard electrostatic nature of atoms being the primary charge carriers in SU. The flow of negative charge to the hydrophobic tails and aliphatic side-chains of amino acid L residues is strongly limited. The lack of significant negative charge on the fatty acid tails shows that, even in its anionic form, SU preserves its amphiphilic structure responsible for its surface and biological activities.

The approximate size of the SU micellar aggregates was estimated using the DFT calculations (Table 4). The micelle diameter (d_{mic}) at the DFT level was approximated as the longest distance between two carbon atoms in optimized molecular structures of the SU homologues. The predicted d_{mic} values increase with the hydrophobic chain length from 3.84 nm for *a*-C_{12} to 4.82 nm for *n*-C_{15}. Hence, the SU micelle diameter can be directly controlled by the number of carbon atoms in the *β*-hydroxy fatty acid chain. A similar phenomenon was observed, for instance, for the homologous series of fluorinated (Matsuoka et al., 2006; Matsuoka et al., 2007) and di-N-oxide surfactants (Lewińska et al., 2012; Lewińska et al., 2014). Although this rule seems to be taken for granted, several exceptions have been reported. For example, the tendency for the micelle diameter to increase with the number of carbon atoms in the aliphatic chain was not observed for divalent cationic surfactants composed of fluorocarbons and double quaternary ammonium groups (Matsuoka et al., 2011).

The predicted d_{mic} values for all isomers of each homologue are noticeably underestimated compared to the DLS results. However, it is important to acknowledge certain limitations when comparing the results of quantum mechanical calculations with DLS measurements. DLS directly measures hydrodynamic quantities, such as translational and/or rotational diffusion coefficients, which are then related to size and shape through theoretical relationships (Pecora, 2000; Lim et al., 2013). As a result, DLS measurements provide hydrodynamic diameter that can be significantly larger than the geometric particle diameter obtained from DFT predictions, due to the inclusion of possible solvation layers, for instance. It is worth noting that particle diameters determined by DLS are frequently larger than those obtained using other experimental techniques (Lim et al., 2013; Souza et al., 2016). In the case of the SU micelles studied here, which were measured in TRIS×HCl buffer (pH = 8.5), the difference between the DFT and DLS diameter is expected to be further magnified due to the incorporation of relatively large, protonated tris(hydroxymethyl)aminomethane molecules into the layer around the micelles to balance the negative charge of aggregating deprotonated surfactin. Additionally, the discrepancy between theory and experiment may also be influenced by the anisotropic shape of the micelles, as we observed their slightly elliptical shape by TEM imaging (Figure 8).

We attempted to estimate aggregation numbers (N_{agg}) at the DFT theory level, assuming a spherical shape of the micellar aggregates, because the divergence from a perfect sphere could not be quantitatively determined. First, the micelle volumes (V_{mic}) were calculated from the equation:

$$V_{mic}{}^{DFT} = \frac{4}{3} \cdot \pi \cdot \left(\frac{1}{2} d_{mic}{}^{DFT}\right)^3 \tag{7}$$

leading to the simple expression for N_{agg}:

$$N_{agg} = \frac{V_{mic}^{DFT}}{V_{mon}^{DFT}} \tag{8}$$

Previously, the molecular volumes of the hydrated monomers (V_{mon}) were computed using numerical Monte Carlo (MC) integration with a density contour of 0.001 au (Ferreira et al., 2010; Lewińska et al., 2012; Lewińska et al., 2014). Although the high accuracy of this procedure has been demonstrated, in this work we used the Marching Tetrahedra algorithm (Lu and Chen, 2012b) for computation of V_{mon} instead of repeated random sampling of MC methods.

We found that the differences between the molecular structures of the peptide ring are insubstantial between different SU homologues and their isomers. Thus, the calculated d_{mic}, V_{mon} and V_{mic} values mainly depend on the fatty acid chain length. As a result, the N_{agg} number is always the highest for the *n*-isomer for each isoform. The number of surfactin molecules building a single micelle is predicted to increase significantly when the fatty acid chain is extended, for instance, from 23 for *i*-C_{12} to 36 for *i*-C_{15}, or from 27 for *n*-C_{12} to 42 for *n*-C_{15}.

To put this result into perspective, we can compare it with the rise in N_{agg} on the number of carbon atoms in the aliphatic chain reported for two-headed single-chain di-N-oxide surfactants of the C_n(DAPANO)$_2$ and C_n-MEDA series (Lewińska et al., 2012; Lewińska et al., 2014). For C_n(DAPANO)$_2$ N_{agg} increases from 33 for n = 10 to 91 for n = 16, while for C_n-MEDA it increases from 49 for n = 10 to 99 for n = 16. The rise in aggregation number for dicephalic di-N-oxide surfactants is significantly greater in comparison with SU. Although these dicephalic surfactants have a relatively large hydrophilic end, they are noticeably smaller and less hydrophilic in comparison with SU. These inimitable structural features of SU result in several unique properties of their aggregate states, such as a lowered aggregate size and aggregation number.

Our theoretical analysis demonstrates that the aggregation numbers for SU micelles are significantly smaller compared to those of typical surfactants, as evidenced by the comparison with C_n(DAPANO)$_2$ and C_n-MEDA in the preceding paragraph. Therefore, it is crucial to compare these theoretical findings with experimental values obtained from small angle neutron scattering (SANS). Shen et al. investigated the SU mixture with varying β-hydroxy fatty acid chains, produced by the strain BBK006 bacteria, and reported an aggregation number of 20 ± 5 (Shen et al., 2009). It is important to note that in the SU mixture used by Shen et al., the dominant homologue was C_{13}. Zou et al. studied the [Glu1, Asp5]-C_{15} isoform from *B. subtilis* HSO121 and found the SU aggregation number to be "unbelievably small" (less than 20), which they considered to be similar to the results of Shen et al. (Zou et al., 2010). A direct comparison between theory and the SANS experiments is difficult due to the influence of experimental conditions such as pH or the presence of various homologues in the SU mixture on N_{agg}. Nevertheless, our DFT calculations, based on the molecular volumes derived from electron density and the micelle diameters obtained from molecular structures of SU molecules, consistently yield small values for N_{agg}. They align well with the experimental results, particularly our prediction of N_{agg} = 27 for *iso*-C_{13}, which closely resembles the N_{agg} = 20 ± 5 reported by Shen et al. (Shen et al., 2009).

3.7 Contact angle assay

The wettability of the solution in relation to the surface with which it is in contact can be determined by measurement of the contact angles (Luner et al., 1996; Zhang et al., 2010). Contact angle is the angle between the contact plane and the tangent line to the droplet derived from the contact point of the three phases, solid, liquid and gas. If the measured value is lower than 90°, it means that the analyzed liquid prefers to develop the surface of contact with a solid, so it has good wetting properties. In the opposite situation, when the angle is higher than 90°, it means that the solution avoids contact with the surface and wetting is weak (Mohammadi et al., 2004; Lamour et al., 2010). For the contact angle assay, two types of surfaces were used, glass (as the hydrophilic one) and polyethylene–PE (as the hydrophobic one) and the results are shown in Figure 10. Concentration of 0.11 mg/mL of SU's homologues was tested in 0.05 M TRIS×HCl (pH = 8.5), and the buffer was measured as the control sample. For PE, the contact angle was reduced to about 50° from 71.4° depending on homologue. This means that SU improves wettability by 30%, which is comparable with sodium dodecyl sulphate, whose minimum contact angle in a water-polyethylene system is between 50° and 60° (Mańko et al., 2016). The strongest effect was recorded for C_{14} resulting in 46.9°, and C_{13} (50.7°), the weakest for C_{12} (74.8°). C_{15} (58.4°) was between them. In the case of glass, the pattern was similar–the strongest effect was measured for C_{14} (33.7°), while C_{13} and C_{15} were not significantly different (39.2° and 40.0°) and C12 (51.2°) was the weakest one. SU's wetting ability in contact with glass can be compared to the Triton-TX165, whose water solution gives minimum contact angle equal to 36° (Szymczyk and Jańczuk, 2008). One would expect that the contact angle values would decrease with increasing force of the surface tension reduction of the homologues, and therefore in the order $C_{12} < C_{13} < C_{14} < C_{15}$. Indeed, the weakest wettability is observed for the C_{12} homologue, but in the case of C_{13}, C_{14} and C_{15}, the recorded differences are small. C_{14} shows the best wetting ability, C_{13} and C_{15} slightly lower. This is consistent with other literature reports, where, for example, the wettability angles for sodium dodecyl sulphate and sodium hexadecyl sulphate (which differ in as many as four carbon atoms) were compared and the same insignificant differences were shown (Zdziennicka et al., 2003). An interesting fact is that the quantitative distribution of homologues in a natural mixture of surfactin correlates with the strength of wetting ability. It can be seen from Figure 1A that the most abundant homologue is C_{14}, then C_{15} and C_{13}, whose quantities are similar. C_{12}, having the weakest wetting properties, is the least abundant. One of the natural functions of SU is an improvement of biofilm formation, which is important in the expansion of *B. subtilis* in the environment (Bais et al., 2004; Leclère et al., 2006; López et al., 2009) High wetting ability can be a crucial parameter for the growth of biofilm and gliding, so the C_{14} homologue as the most effective agent is produced in the highest quantities. SU is produced by bacteria species, including some strains known to exhibit gliding motility. Gliding motility is a form of bacterial movement that allows cells to move smoothly and rapidly along a solid surface without the use of flagella. The mechanism of gliding is still not completely understood. One of the proposed mechanisms is the "slime propulsion" model, which suggests that gliding motility is driven by the flow of a slimy

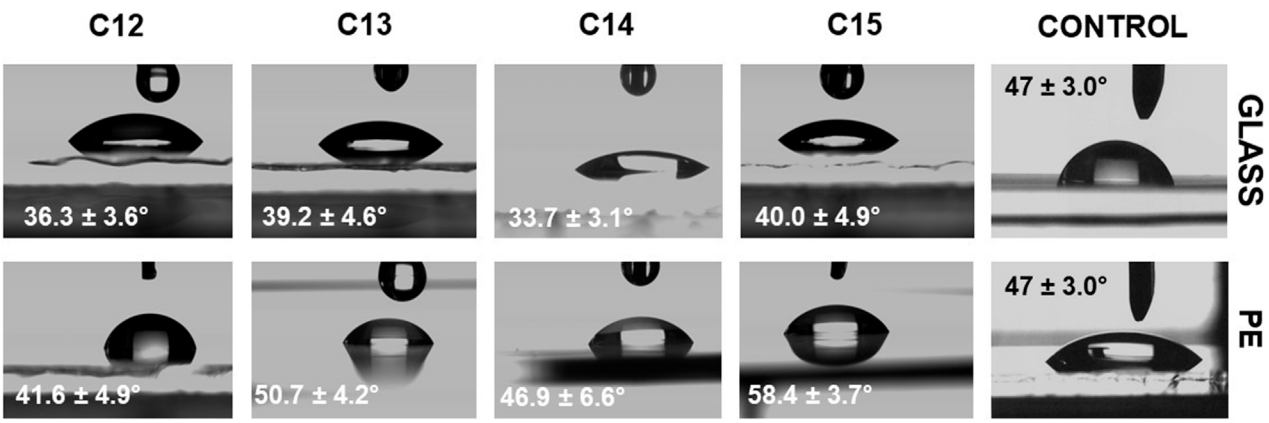

FIGURE 10
Contact angle assay results.

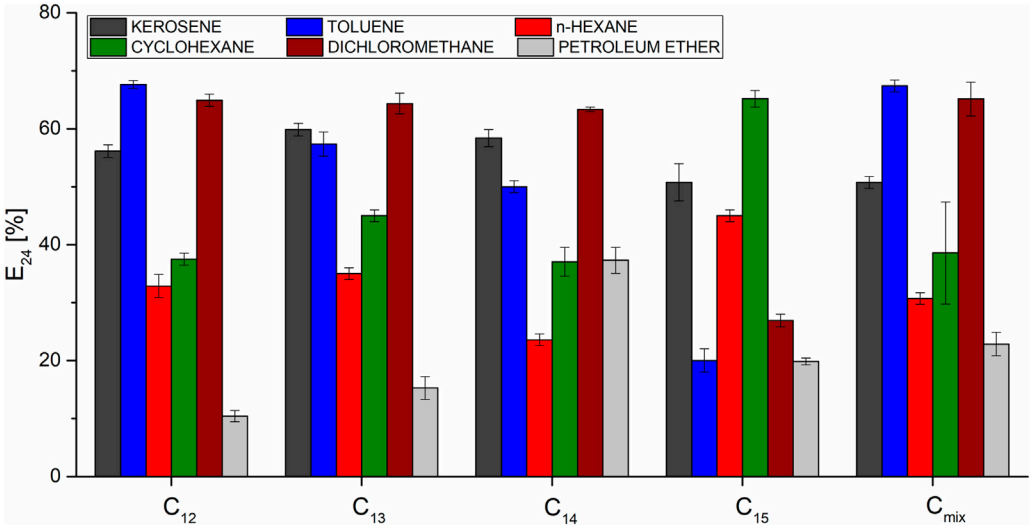

FIGURE 11
Emulsification indexes determined for SU homologues.

extracellular matrix that is produced by the bacteria where contact angle and surface tension may be a partial driving force of the flow.

The results indicate that SU can be effectively used as a wetting agent, with its mixture showing similar efficacy to that of the pure homologues when applied immediately after microbial production. Moreover, the low toxicity, biodegradability, and biocompatibility of SU (de Oliveira et al., 2017) make it a promising candidate for various applications, such as the removal of hydrophobic environmental pollutants (Mulligan, 2005; Wang et al., 2020; Meena et al., 2021).

3.8 Emulsification indexes (E_{24})

In order to compare emulsification ability of particular homologues, emulsification indexes were determined for different hydrophobic phases. The tested substances were kerosene, toluene, *n*-hexane, cyclohexane, dichloromethane and petroleum ether. Results obtained for the homologues (Figure 11) completely disagreed with their measured surface tension reduction abilities, which is consistent with previous research done on biosurfactants (Cooper and Goldenberg, 1987; Menezes Bento et al., 2005). In addition, the one strongest homologue was not observed. The intensity of emulsification was different for the tested hydrophobic phases and, for example, C_{14} was the most efficient emulsifier in the case of petroleum ether (37.3%) but the worst one in the case of *n*-hexane (23.6%) and cyclohexane (27.5%). C_{15} was the best emulsifier for *n*-hexane (45.0%) and cyclohexane (65.2%), and worst in the case of kerosene (50.8%), toluene (20.0%) and dichloromethane (26.9%). The best overall emulsification strength of SU was observed for kerosene (about 60%), toluene, cyclohexane

and dichloromethane (about 70%). Emulsification indexes of *n*-hexane and petroleum ether were the worst. E_{24} determined for the native mixture of homologues (non-separated sample) was not the average value of its ingredients. This means that contributions of particular homologues to the overall effect is not equal. However, several dependencies have been observed. Petroleum ether is a fraction of oil distilled in the temperature range of 40°C–60°C and forms the mixture of pentane and hexane isomers. In relation to this substance, C_{15} shows a much higher EI24 than the other homologues, while showing a much lower ability to homogenize toluene. This means that the length of the homologue may be important for the homogenization of aliphatic and aromatic compounds - shorter ones are more effective against aromatic hydrocarbons. Kerosene, which is distilled from oil at temperatures of 170°C–250°C, contains mainly C_{12}-C_{15} alkanes and is much more effectively emulsified by all surfactin samples than petroleum ether. This means that surfactin has better emulsifying properties than alkanes with long hydrocarbon chains. Taking into account its structure, it makes sense, because the interaction with non-polar phases is mediated by hydrophobic chains of β-hydroxy fatty acids, the lengths of which are closer to those of kerosene than petroleum ether. Short hydrophobic chains are present in the amino acid ring, but a partial electrostatic charge bearing peptide bond and D and E residues prevent them from interacting with hydrophobic substances. There is also a noticeable difference between the group C_{12}-C_{14} and C_{15} in the E_{24} for dichloromethane, shorter homologues show a higher efficiency against halogen derivatives. In addition, for all homologues, a better ability to emulsify cyclohexane than hexane is observed, which means that, in general, surfactin is more likely to form an emulsion from cyclic hydrocarbons. The known fact is that SU homologue composition strongly depends on the environmental factors (Bartal et al., 2018). Emulsification of nonpolar substances is the way to make them more bioavailable for bacteria. It is possible that depending on the surrounding's properties, *Bacillus* produces homologues with different compositions in order to emulsify hydrophobic materials since they have various emulsifying potentials.

4 Conclusion

Flash chromatography has proven to be the most effective method for separating SU homologues. Using this technique, we obtained C_{13}, C_{14}, and C_{15} homologues with yields of over 100 mg from a single injection. We also isolated small amounts of C_{12} for comparative analysis. LC-MS and GC-MS analyses confirmed that the obtained compound samples were homologue pairs. Using Gibbs isotherms, we compared the surface tension reduction ability and *CMC* values, and found that C_{15} was the strongest surfactant molecule, with increasing surface activity observed with increasing homologue length. TEM, DLS, and DFT techniques were used to describe the micellization behavior, revealing that the less spherical the micelle, the more carbon atoms present in the homologue, with hydrodynamic diameters ranging from 4.7 to 5.7 nm between C_{12} and C_{15}. Computational data obtained with DFT showed that SU has a very low aggregation number. Based on isosurface maps, we concluded that SU molecules have a large polar surface area and a relatively small hydrophobic moiety, suggesting that SU, when aggregating, contributes more to the formation of the micelle surface than to its internal volume.

The usefulness of surfactants relates to micelle formation, as these aggregates are responsible for the washing effect. A low aggregation number means that fewer molecules are necessary to form a micelle, and thus, a surfactant with a lower aggregation number at the same concentration is a more powerful washing agent compared to one with a high aggregation number. To describe the functional properties of the homologues, we investigated contact angles and emulsification indexes, finding that the strength of surface reduction did not consistently correlate with wetting ability or emulsification capability. C_{14} was the most abundant homologue in the natural mixture and the best wetting agent according to our contact angle assay results. This homologue is likely produced in abundance due to its positive impact on *Bacillus* biofilm formation. However, the contribution to gliding motility is not the only function of SU. *Bacillus* can secrete SU into the environment to emulsify hydrophobic substances and make them more bioavailable. From the E_{24} analysis, we observed that there is no consistent rule among homologues in emulsification strength. The peptide chain enables a multitude of interactions with other compounds, and different homologues have various emulsifying efficiencies with tested substances, indicating that an SU mixture containing small amounts of various homologues improves *Bacillus*' ability to cope with environmental conditions due to better emulsifying ability than a single structure.

This point of view allows us to understand the significance of SU for the producing organism better. It appears that SU is not only one of the strongest known biosurfactants with high utility value but also a powerful tool for the succession of bacteria in its environment. The published methodology, based on SU, can be applied to other similar structures of cyclic lipopeptides, allowing for a better understanding of their structure-properties relationship.

Data availability statement

The raw data supporting the conclusion of this article will be made available by the authors, without undue reservation.

Author contributions

Conceptualization, AL; methodology, MB, AL, MW, and MŁ; investigation, MB, AL, and MW; formal analysis, MB, AL, MW, and MŁ; resources, MB, AL, MW, AD, MŁ; data curation, AL; writing—original draft preparation, MB and AL; writing—review and editing, AL and MŁ; visualization, MB and AL; supervision, AL; project administration, AL and MŁ; funding acquisition, AL and MŁ. All authors contributed to the article and approved the submitted version.

Funding

Financial support from the statutory activity of subsidy from the Polish Ministry of Science and Higher Education for the Faculty of Chemistry and Faculty of Biotechnology of the University of

Wroclaw is gratefully acknowledged. The computations were performed using computers and software licenses of the Wrocław Centre for Networking and Supercomputing (Grant No. 47). Work partially financed by POIR.01.01.01-00-0729/19 and POIR. POIR.01.01.01-00-1433/19.

Conflict of interest

Authors MB, AL and AG carried out part of the research in InventionBio and OnlyBio as part of the research projects POIR.01.01.01-00-0729/19 and POIR.01.01.01-00-1433/19.

The remaining authors declare that the research was conducted in the absence of any commercial or financial relationships that could be construed as a potential conflict of interest.

Publisher's note

Supplementary material

The Supplementary Material for this article can be found online at: https://www.frontiersin.org/articles/10.3389/fbioe.2023.1211319/full#supplementary-material

References

Abe, M. (Editor) (2019). *Measurement techniques and practices of colloid and interface phenomena* (Singapore: Springer Singapore).

Allouche, A.-R. (2011). Gabedit-A graphical user interface for computational chemistry softwares. *J. Comput. Chem.* 32 (1), 174–182. doi:10.1002/jcc.21600

Arutchelvi, J., Bhaduri, S., Uppara, P. V., and Doble, M. (2009). Production and characterization of biosurfactant from Bacillus subtilis YB7. *J. Appl. Sci.* 9 (17), 3151–3155. doi:10.3923/jas.2009.3151.3155

Arutchelvi, J., Sangeetha, J., Philip, J., and Doble, M. (2014). Self-assembly of surfactin in aqueous solution: Role of divalent counterions. *Colloids Surfaces B Biointerfaces* 116, 396–402. doi:10.1016/j.colsurfb.2013.12.034

Bader, R. F. W., Carroll, M. T., Cheeseman, J. R., and Chang, C. (1987). Properties of atoms in molecules: Atomic volumes. *J. Am. Chem. Soc.* 109 (26), 7968–7979. doi:10.1021/ja00260a006

Bais, H. P., Fall, R., and Vivanco, J. M. (2004). Biocontrol of *Bacillus subtilis* against infection of arabidopsis roots by *Pseudomonas syringae* is facilitated by biofilm formation and surfactin production. *Plant Physiol.* 134 (1), 307–319. doi:10.1104/pp.103.028712

Barone, V., and Cossi, M. (1998). Quantum calculation of molecular energies and energy gradients in solution by a conductor solvent model. *J. Phys. Chem. A* 102 (11), 1995–2001. doi:10.1021/jp9716997

Bartal, A., Vigneshwari, A., Bóka, B., Vörös, M., Takács, I., Kredics, L., et al. (2018). Effects of different cultivation parameters on the production of surfactin variants by a Bacillus subtilis strain. *Molecules* 23 (10), 2675. doi:10.3390/molecules23102675

Becke, A. D. (1988). Density-functional exchange-energy approximation with correct asymptotic behavior. *Phys. Rev. A* 38 (6), 3098–3100. doi:10.1103/physreva.38.3098

Becke, A. D. (1993). Density-functional thermochemistry. III. The role of exact exchange. *J. Chem. Phys.* 98 (7), 5648–5652. doi:10.1063/1.464913

Bezza, F. A., and Chirwa, E. M. N. (2015). Production and applications of lipopeptide biosurfactant for bioremediation and oil recovery by Bacillus subtilis CN2. *Biochem. Eng. J.* 101, 168–178. doi:10.1016/j.bej.2015.05.007

Bidlingmeyer, B. A., Cohen, S. A., and Tarvin, T. L. (1984). Rapid analysis of amino acids using pre-column derivatization. *J. Chromatogr. B Biomed. Sci. Appl.* 336 (1), 93–104. doi:10.1016/s0378-4347(00)85133-6

Bruner, S. D., Weber, T., Kohli, R. M., Schwarzer, D., Marahiel, M. A., Walsh, C. T., et al. (2002). Structural basis for the cyclization of the lipopeptide antibiotic surfactin by the thioesterase domain SrfTE. *Structure* 10 (3), 301–310. doi:10.1016/s0969-2126(02)00716-5

Cao, T.-T., Cui, H., Zhou, D.-D., Ren, X., and Cui, C.-W. (2022). Degradation mechanism of BPA under VUV irradiation: Efficiency contribution and DFT calculations. *Environ. Sci. Pollut. Res.* 17, 12813–12824. doi:10.1007/s11356-022-22893-1

Cooper, D. G., and Goldenberg, B. G. (1987). Surface-active agents from two *Bacillus* species. *Appl. Environ. Microbiol.* 53 (2), 224–229. doi:10.1128/aem.53.2.224-229.1987

Ćwieląg-Piasecka, I., Witwicki, M., Jerzykiewicz, M., and Jezierska, J. (2017). Can carbamates undergo radical oxidation in the soil environment? A case study on carbaryl and carbofuran. *Environ. Sci. Technol.* 51 (24), 14124–14134. doi:10.1021/acs.est.7b03386

de Oliveira, D. W. F., Cara, A. B., Lechuga-Villena, M., García-Román, M., Melo, V. M. M., Gonçalves, L. R. B., et al. (2017). Aquatic toxicity and biodegradability of a surfactant produced by *Bacillus subtilis* ICA56. *J. Environ. Sci. Health, Part A* 52 (2), 174–181. doi:10.1080/10934529.2016.1240491

DeepikaVerma Sharma, S., and Vashishtha, M. (2022). Evaluation of optimized molecular structure-antimicrobial and antioxidant efficacy relationship of Schiff bases. *Environ. Sci. Pollut. Res.* 19, 20874–20886. doi:10.1007/s11356-022-23633-1

Durán-Álvarez, A., Maldonado-Domínguez, M., González-Antonio, O., Durán-Valencia, C., Romero-Ávila, M., Barragán-Aroche, F., et al. (2016). Experimental–theoretical approach to the adsorption mechanisms for anionic, cationic, and zwitterionic surfactants at the calcite–water interface. *Langmuir* 32 (11), 2608–2616. doi:10.1021/acs.langmuir.5b04151

Ferreira, T. L., Sato, B. M., el Seoud, O. A., and Bertotti, M. (2010). Application of microelectrode voltammetry to study the properties of surfactant solutions: Alkyltrimethylammonium bromides. *J. Phys. Chem. B* 114 (2), 857–862. doi:10.1021/jp909655y

Goldburg, W. I. (1999). Dynamic light scattering. *Am. J. Phys.* 67 (12), 1152–1160. doi:10.1119/1.19101

Gonzalez-Castro, M. J., Lopez-Hernandez, J., Simal-Lozano, J., and Oruna-Concha, M. J. (1997). Determination of amino acids in green beans by derivatization with phenylisothiocianate and high-performance liquid chromatography with ultraviolet detection. *J. Chromatogr. Sci.* 35 (4), 181–185. doi:10.1093/chromsci/35.4.181

Gorb, L., Ilchenko, M., and Leszczynski, J. (2022). Decomposition of 2,4,6-trinitrotoluene (TNT) and 5-nitro-2,4-dihydro-3H-1,2,4-triazol-3-one (NTO) by Fe13O13 nanoparticle: Density functional theory study. *Environ. Sci. Pollut. Res.* 29 (45), 68522–68531. doi:10.1007/s11356-022-20547-w

Gracia, C. A., Gómez-Barreiro, S., González-Pérez, A., Nimo, J., and Rodriguez, J. R. (2004). Static and dynamic light-scattering studies on micellar solutions of alkyldimethylbenzylammonium chlorides. *J. Colloid Interface Sci.* 276 (2), 408–413. doi:10.1016/j.jcis.2004.04.002

Grangemard, I., Peypoux, F., Wallach, J., Das, B. C., Labbé, H., Caille, A., et al. (1997). Lipopeptides with improved properties: Structure by NMR, purification by HPLC and structure–activity relationships of new isoleucyl-rich surfactins. *J. Peptide Sci.* 3 (2), 145–154. doi:10.1002/(sici)1099-1387(199703)3:2<145:aid-psc96>3.0.co;2-y

Grimme, S., Antony, J., Ehrlich, S., and Krieg, H. (2010). A consistent and accurate *ab initio* parametrization of density functional dispersion correction (DFT-D) for the 94 elements H-Pu. *J. Chem. Phys.* 132 (15), 154104. doi:10.1063/1.3382344

Grimme, S., Ehrlich, S., and Goerigk, L. (2011). Effect of the damping function in dispersion corrected density functional theory. *J. Comput. Chem.* 32 (7), 1456–1465. doi:10.1002/jcc.21759

Han, Y., Huang, X., Cao, M., and Wang, Y. (2008). Micellization of surfactin and its effect on the aggregate conformation of amyloid β(1-40). *J. Phys. Chem. B* 112 (47), 15195–15201. doi:10.1021/jp805966x

Horng, Y. B., Yu, Y. H., Dybus, A., Hsiao, F. S. H., and Cheng, Y. H. (2019). Antibacterial activity of Bacillus species-derived surfactin on Brachyspira hyodysenteriae and *Clostridium perfringens*. *Amb. Express* 9 (1), 188. doi:10.1186/s13568-019-0914-2

Hu, F., Liu, Y., and Li, S. (2019). Rational strain improvement for surfactin production: Enhancing the yield and generating novel structures. *Microb. Cell. Factories* 18 (1), 42. doi:10.1186/s12934-019-1089-x

Ishigami, Y., Osman, M., Nakahara, H., Sano, Y., Ishiguro, R., and Matsumoto, M. (1995). Significance of β-sheet formation for micellization and surface adsorption of

surfactin. *Colloids Surfaces B Biointerfaces* 4 (6), 341–348. doi:10.1016/0927-7765(94)01183-6

Jajor, P., Piłakowska-Pietras, D., Krasowska, A., and Łukaszewicz, M. (2016). Surfactin analogues produced by Bacillus subtilis strains grown on rapeseed cake. *J. Mol. Struct.* 1126, 141–146. doi:10.1016/j.molstruc.2016.02.014

Jauregi, P., Coutte, F., Catiau, L., Lecouturier, D., and Jacques, P. (2013). Micelle size characterization of lipopeptides produced by B. subtilis and their recovery by the two-step ultrafiltration process. *Sep. Purif. Technol.* 104, 175–182. doi:10.1016/j.seppur.2012.11.017

Kim, K. M., Lee, J. Y., Kim, C. K., and Kang, J. S. (2009). Isolation and characterization of surfactin produced by Bacillus polyfermenticus KJS-2. *Archives Pharmacal Res.* 32 (5), 711–715. doi:10.1007/s12272-009-1509-2

Knoblich, A., Matsumoto, M., Ishiguro, R., Murata, K., Fujiyoshi, Y., Ishigami, Y., et al. (1995). Electron cryo-microscopic studies on micellar shape and size of surfactin, an anionic lipopeptide. *Colloids Surfaces B Biointerfaces* 5 (1–2), 43–48. doi:10.1016/0927-7765(95)01207-y

Kossmann, S., and Neese, F. (2009). Comparison of two efficient approximate Hartee–Fock approaches. *Chem. Phys. Lett.* 481 (4–6), 240–243. doi:10.1016/j.cplett.2009.09.073

Kowall, M., Vater, J., Kluge, B., Stein, T., Franke, P., and Ziessow, D. (1998). Separation and characterization of surfactin isoforms produced byBacillus subtilisOKB 105. *J. Colloid Interface Sci.* 204 (1), 1–8. doi:10.1006/jcis.1998.5558

Kracht, M., Rokos, H., Özel, M., Kowall, M., Pauli, G., and Vater, J. (1999). Antiviral and hemolytic activities of surfactin isoforms and their methyl ester derivatives. *J. Antibiotics* 52 (7), 613–619. doi:10.7164/antibiotics.52.613

Lamour, G., Hamraoui, A., Buvailo, A., Xing, Y., Keuleyan, S., Prakash, V., et al. (2010). Contact angle measurements using a simplified experimental setup. *J. Chem. Educ.* 87 (12), 1403–1407. doi:10.1021/ed100468u

Leclère, V., Marti, R., Béchet, M., Fickers, P., and Jacques, P. (2006). The lipopeptides mycosubtilin and surfactin enhance spreading of Bacillus subtilis strains by their surface-active properties. *Archives Microbiol.* 186 (6), 475–483. doi:10.1007/s00203-006-0163-z

Lee, C., Yang, W., and Parr, R. G. (1988). Development of the Colle-Salvetti correlation-energy formula into a functional of the electron density. *Phys. Rev. B* 37 (2), 785–789. doi:10.1103/physrevb.37.785

Lewińska, A., Domżał-Kędzia, M., Jaromin, A., and Łukaszewicz, M. (2020). Nanoemulsion stabilized by safe surfactin from Bacillus subtilis as a multifunctional, custom-designed smart delivery system. *Pharmaceutics* 12 (10), 953–1021. doi:10.3390/pharmaceutics12100953

Lewińska, A., Domżał-Kędzia, M., Kierul, K., Bochynek, M., Pannert, D., Nowaczyk, P., et al. (2021c). Targeted hybrid nanocarriers as a system enhancing the skin structure. *Mol. (Basel, Switz.* 26 (4), 1063–1120. doi:10.3390/molecules26041063

Lewińska, A., Domżał-Kędzia, M., Maciejczyk, E., Łukaszewicz, M., and Bazylińska, U. (2021b). Design and engineering of "green" nanoemulsions for enhanced topical delivery of bakuchiol achieved in a sustainable manner: A novel eco-friendly approach to bioretinol. *Int. J. Mol. Sci.* 22 (18), 10091. doi:10.3390/ijms221810091

Lewińska, A., Domżał-Kędzia, M., Wójtowicz, K., and Bazylińska, U. (2022). Surfactin-stabilized poly(D,L-lactide) nanoparticles for potential skin application. *Colloids Surfaces A Physicochem. Eng. Aspects* 648, 129216. doi:10.1016/j.colsurfa.2022.129216

Lewińska, A., Kulbacka, J., Domżał-Kędzia, M., and Witwicki, M. (2021a). Antiradical properties of N-oxide surfactants—two in one. *Int. J. Mol. Sci.* 22 (15), 8040. doi:10.3390/ijms22158040

Lewińska, A., Witwicki, M., Bazylińska, U., Jezierski, A., and Wilk, K. A. (2014). Aggregation behavior of dicephalic di-N-oxide surfactants in aqueous solution: Experimental and computational approaches. *Colloids Surfaces A Physicochem. Eng. Aspects* 442, 34–41. doi:10.1016/j.colsurfa.2013.03.006

Lewińska, A., Witwicki, M., Frąckowiak, R., Jezierski, A., and Wilk, K. A. (2012). Experimental and theoretical approach to aggregation behavior of new di- *N* -oxide surfactants in an aquatic environment. *J. Phys. Chem. B* 116 (49), 14324–14332. doi:10.1021/jp306282m

Li, Y., Ye, R.-Q., and Mu, B.-Z. (2009b). Influence of sodium ions on micelles of surfactin-C16 in solution. *J. Surfactants Deterg.* 12 (1), 31–36. doi:10.1007/s11743-008-1094-2

Li, Y., Zou, A.-H., Ye, R.-Q., and Mu, B.-Z. (2009a). Counterion-induced changes to the micellization of surfactin-C $_{16}$ aqueous solution. *J. Phys. Chem. B* 113 (46), 15272–15277. doi:10.1021/jp9062862

Lim, J., Yeap, S. P., Che, H. X., and Low, S. C. (2013). Characterization of magnetic nanoparticle by dynamic light scattering. *Nanoscale Res. Lett.* 8 (1), 381. doi:10.1186/1556-276x-8-381

Liu, J.-F., Mbadinga, S., Yang, S.-Z., Gu, J.-D., and Mu, B.-Z. (2015). Chemical structure, property and potential applications of biosurfactants produced by Bacillus subtilis in petroleum recovery and spill mitigation. *Int. J. Mol. Sci.* 16 (3), 4814–4837. doi:10.3390/ijms16034814

Liu, X., Yang, S., and Mu, B. (2008). Isolation and characterization of a C $_{12}$ -lipopeptide produced by *Bacillus subtilis* HSO 121. *J. Peptide Sci.* 14 (7), 864–875. doi:10.1002/psc.1017

Liu, Z., Lu, T., and Chen, Q. (2021). Intermolecular interaction characteristics of the all-carboatomic ring, cyclo[18]carbon: Focusing on molecular adsorption and stacking. *Carbon* 171, 514–523. doi:10.1016/j.carbon.2020.09.048

López, D., Vlamakis, H., Losick, R., and Kolter, R. (2009). Cannibalism enhances biofilm development in *Bacillus subtilis*. *Mol. Microbiol.* 74 (3), 609–618. doi:10.1111/j.1365-2958.2009.06882.x

Lu, T., and Chen, F. (2012a). Multiwfn: A multifunctional wavefunction analyzer. *J. Comput. Chem.* 33 (5), 580–592. doi:10.1002/jcc.22885

Lu, T., and Chen, F. (2012b). Quantitative analysis of molecular surface based on improved Marching Tetrahedra algorithm. *J. Mol. Graph. Model.* 38, 314–323. doi:10.1016/j.jmgm.2012.07.004

Luner, P. E., Babu, S. R., and Mehta, S. C. (1996). Wettability of a hydrophobic drug by surfactant solutions. *Int. J. Pharm.* 128 (1–2), 29–44. doi:10.1016/0378-5173(95)04208-3

Maget-Dana, R., and Ptak, M. (1995). Interactions of surfactin with membrane models. *Biophysical J.* 68 (5), 1937–1943. doi:10.1016/s0006-3495(95)80370-x

Matsuoka, K., Chiba, N., Yoshimura, T., and Takeuchi, E. (2011). Effect of double quaternary ammonium groups on micelle formation of partially fluorinated surfactant. *J. Colloid Interface Sci.* 356 (2), 624–629. doi:10.1016/j.jcis.2011.01.030

Matsuoka, K., Yonekawa, A., Ishii, M., Honda, C., Endo, K., Moroi, Y., et al. (2006). Micellar size, shape and counterion binding of N-(1,1-Dihydroperfluoroalkyl)-N,N,N-trimethylammonium chloride in aqueous solutions. *Colloid Polym. Sci.* 285 (3), 323–330. doi:10.1007/s00396-006-1574-8

Matsuoka, K., Yoshimura, T., Shikimoto, T., Hamada, J., Yamawaki, M., Honda, C., et al. (2007). Molecular aggregates of partially fluorinated quaternary ammonium salt gemini surfactants. *Langmuir* 23 (22), 10990–10994. doi:10.1021/la701525c

Mańko, D., Zdziennicka, A., Krawczyk, J., and Jańczuk, B. (2016). Wettability prediction of such polymers as polyethylene and polytetrafluoroethylene by aqueous solutions of classical surfactants and biosurfactants. *Colloids Surfaces A Physicochem. Eng. Aspects* 506, 409–415. doi:10.1016/j.colsurfa.2016.06.061

Meena, K. R., Dhiman, R., Singh, K., Kumar, S., Sharma, A., Kanwar, S. S., et al. (2021). Purification and identification of a surfactin biosurfactant and engine oil degradation by Bacillus velezensis KLP2016. *Microb. Cell. Factories* 20 (1), 26. doi:10.1186/s12934-021-01519-0

Menezes Bento, F., de Oliveira Camargo, F. A., Okeke, B. C., and Frankenberger, W. T. (2005). Diversity of biosurfactant producing microorganisms isolated from soils contaminated with diesel oil. *Microbiol. Res.* 160 (3), 249–255. doi:10.1016/j.micres.2004.08.005

Mnif, I., Mnif, S., Sahnoun, R., Maktouf, S., Ayedi, Y., Ellouze-Chaabouni, S., et al. (2015). Biodegradation of diesel oil by a novel microbial consortium: Comparison between co-inoculation with biosurfactant-producing strain and exogenously added biosurfactants. *Environ. Sci. Pollut. Res.* 22 (19), 14852–14861. doi:10.1007/s11356-015-4488-5

Mohammadi, R., Wassink, J., and Amirfazli, A. (2004). Effect of surfactants on wetting of super-hydrophobic surfaces. *Langmuir* 20 (22), 9657–9662. doi:10.1021/la049268k

Morán, A. C., Olivera, N., Commendatore, M., Esteves, J. L., and Siñeriz, F. (2000). Enhancement of hydrocarbon wastebiodegradation by addition of a biosurfactantfrom Bacillus subtilis O9. *Biodegradation* 11 (1), 65–71. doi:10.1023/a:1026513312169

Mulligan, C. N. (2005). Environmental applications for biosurfactants. *Environ. Pollut.* 133 (2), 183–198. doi:10.1016/j.envpol.2004.06.009

Ndlovu, T., Khan, S., and Khan, Wesaal. (2016). Distribution and diversity of biosurfactant-producing bacteria in a wastewater treatment plant. *Environ. Sci. Pollut. Res.* 23 (10), 9993–10004. doi:10.1007/s11356-016-6249-5

Neese, F., Ames, W., Christian, G., Kampa, M., Liakos, D. G., Pantazis, D. A., et al. (2010). Dealing with complexity in open-shell transition metal chemistry from a theoretical perspective: Reaction pathways, bonding, spectroscopy, and magnetic properties. *Adv. Inorg. Chem.* 62, 301–349. doi:10.1016/S0898-8838(10)62008-9

Neese, F. (2003). An improvement of the resolution of the identity approximation for the formation of the Coulomb matrix. *J. Comput. Chem.* 24 (14), 1740–1747. doi:10.1002/jcc.10318

Neese, F. (2022). Software update: The ORCA program system—version 5.0. *WIREs Comput. Mol. Sci.* 12 (5). doi:10.1002/wcms.1606

Neese, F. (2012). The ORCA program system. *WIREs Comput. Mol. Sci.* 2 (1), 73–78. doi:10.1002/wcms.81

Neese, F., Wennmohs, F., Becker, U., and Riplinger, C. (2020). The ORCA quantum chemistry program package. *J. Chem. Phys.* 152 (22), 224108. doi:10.1063/5.0004608

Neese, F., Wennmohs, F., Hansen, A., and Becker, U. (2009). Efficient, approximate and parallel Hartree–Fock and hybrid DFT calculations. A 'chain-of-spheres' algorithm for the Hartree–Fock exchange. *Chem. Phys.* 356 (1–3), 98–109. doi:10.1016/j.chemphys.2008.10.036

O'Boyle, N. M., Banck, M., James, C. A., Morley, C., Vandermeersch, T., and Hutchison, G. R. (2011). Open Babel: An open chemical toolbox. *J. Cheminformatics* 3 (1), 33. doi:10.1186/1758-2946-3-33

Parthipan, P., Preetham, E., Machuca, L. L., Rahman, P. K. S. M., Murugan, K., and Rajasekar, A. (2017). Biosurfactant and degradative enzymes mediated crude oil degradation by bacterium Bacillus subtilis A1. *Front. Microbiol.* 8, 193. doi:10.3389/fmicb.2017.00193

Pecora, R. (2000). Dynamic light scattering measurement of nanometer particles in liquids. *J. Nanoparticle Res.* 2 (2), 123–131. doi:10.1023/a:1010067107182

Perdew, J. P. (1986). Density-functional approximation for the correlation energy of the inhomogeneous electron gas. *Phys. Rev. B* 33 (12), 8822–8824. doi:10.1103/physrevb.33.8822

Peypoux, F., Bonmatin, J.-M., Labbe, H., Das, B. C., Ptak, M., and Michel, G. (1991). Isolation and characterization of a new variant of surfactin, the [Val7]surfactin. *Eur. J. Biochem.* 202 (1), 101–106. doi:10.1111/j.1432-1033.1991.tb16349.x

Qin, W.-Q., Fei, D., Zhou, L., Guo, Y.-J., An, S., Gong, O.-H., et al. (2023). A new surfactin-C $_{17}$ produced by *Bacillus subtilis* TD7 with a low critical micelle concentration and high biological activity. *New J. Chem.* 47 (16), 7604–7612. doi:10.1039/d3nj00123g

Rodríguez-Blanco, L. A. J., Ocampo-Pérez, R., Gómez-Durán, C. F. A., Mojica-Sánchez, J. P., and Razo-Hernández, R. S. (2020). Removal of sulfamethoxazole, sulfadiazine, and sulfamethazine by UV radiation and HO· and SO4·− radicals using a response surface model and DFT calculations. *Environ. Sci. Pollut. Res.* 27 (33), 41609–41622. doi:10.1007/s11356-020-10071-0

Seydlová, G., and Svobodová, J. (2008). Review of surfactin chemical properties and the potential biomedical applications. *Central Eur. J. Med.* 3 (2), 123–133. doi:10.2478/s11536-008-0002-5

Shen, H.-H., Thomas, R. K., Chen, C.-Y., Darton, R. C., Baker, S. C., and Penfold, J. (2009). Aggregation of the naturally occurring lipopeptide, surfactin, at interfaces and in solution: An unusual type of surfactant? *Langmuir* 25 (7), 4211–4218. doi:10.1021/la802913x

Shen, H.-H., Thomas, R. K., Penfold, J., and Fragneto, G. (2010). Destruction and solubilization of supported phospholipid bilayers on silica by the biosurfactant surfactin. *Langmuir* 26 (10), 7334–7342. doi:10.1021/la904212x

Singh, A. K., and Cameotra, S. S. (2013). Efficiency of lipopeptide biosurfactants in removal of petroleum hydrocarbons and heavy metals from contaminated soil. *Environ. Sci. Pollut. Res.* 20 (10), 7367–7376. doi:10.1007/s11356-013-1752-4

Souza, T. G. F., Ciminelli, V. S. T., and Mohallem, N. D. S. (2016). A comparison of TEM and DLS methods to characterize size distribution of ceramic nanoparticles. *J. Phys. Conf. Ser.* 733, 012039. doi:10.1088/1742-6596/733/1/012039

Stephens, P. J., Devlin, F. J., Ashvar, C. S., Chabalowski, C. F., and Frisch, M. J. (1994). Theoretical calculation of vibrational circular dichroism spectra. *Faraday Discuss.* 99, 103. doi:10.1039/fd9949900103

Stetefeld, J., McKenna, S. A., and Patel, T. R. (2016). Dynamic light scattering: A practical guide and applications in biomedical sciences. *Biophys. Rev.* 8 (4), 409–427. doi:10.1007/s12551-016-0218-6

Sun, D., Liao, J., Sun, L., Wang, Y., Liu, Y., Deng, Q., et al. (2019). Effect of media and fermentation conditions on surfactin and iturin homologues produced by Bacillus natto NT-6: LC–MS analysis. *Amb. Express* 9 (1), 120. doi:10.1186/s13568-019-0845-y

Szymczyk, K., and Jańczuk, B. (2008). Wettability of a glass surface in the presence of two nonionic surfactant mixtures. *Langmuir* 24 (15), 7755–7760. doi:10.1021/la8008078

Tang, J.-S., Zhao, F., Gao, H., Dai, Y., Yao, Z.-H., Hong, K., et al. (2010). Characterization and online detection of surfactin isomers based on HPLC-MSn analyses and their inhibitory effects on the overproduction of nitric oxide and the release of TNF-α and IL-6 in LPS-induced macrophages. *Mar. Drugs* 8 (10), 2605–2618. doi:10.3390/md8102605

Traube, I. (1940). The earliest history of capillary chemistry. *J. Chem. Educ.* 17 (7), 324. doi:10.1021/ed017p324

Ueno, M., Takasawa, Y., Miyashige, H., Tabata, Y., and Meguro, K. (1981). Effects of alkyl chain length on surface and micellar properties of octaethyleneglycol-n alkyl ethers. *Colloid Polym. Sci.* 259 (7), 761–766. doi:10.1007/bf01419322

Varadaraj, R., Bock, J., Zushma, S., and Brons, N. (1992). Influence of hydrocarbon chain branching on interfacial properties of sodium dodecyl sulfate. *Langmuir* 8 (1), 14–17. doi:10.1021/la00037a004

Varga, Z., Fehér, B., Kitka, D., Wacha, A., Bóta, A., Berényi, S., et al. (2020). Size measurement of extracellular vesicles and synthetic liposomes: The impact of the hydration shell and the protein corona. *Colloids Surfaces B Biointerfaces* 192, 111053. doi:10.1016/j.colsurfb.2020.111053

Vollenbroich, D., Özel, M., Vater, J., Kamp, R. M., and Pauli, G. (1997). Mechanism of inactivation of enveloped viruses by the biosurfactant surfactin from Bacillus subtilis. *Biologicals* 25 (3), 289–297. doi:10.1006/biol.1997.0099

Wang, X., Cai, T., Wen, W., Ai, J., Ai, J., Zhang, Z., et al. (2020). Surfactin for enhanced removal of aromatic hydrocarbons during biodegradation of crude oil. *Fuel* 267, 117272. doi:10.1016/j.fuel.2020.117272

Ward, A. F. H. (1946). Thermodynamics of monolayers on solutions. I. The theoretical significance of Traube's rule. *Trans. Faraday Soc.* 42, 399. doi:10.1039/tf9464200399

Weigend, F. (2006). Accurate Coulomb-fitting basis sets for H to Rn. *Phys. Chem. Chem. Phys.* 8 (9), 1057. doi:10.1039/b515623h

Weigend, F., and Ahlrichs, R. (2005). Balanced basis sets of split valence, triple zeta valence and quadruple zeta valence quality for H to Rn: Design and assessment of accuracy. *Phys. Chem. Chem. Phys.* 7 (18), 3297. doi:10.1039/b508541a

Wen, C. Y., Yin, Z. G., Wang, K. X., Chen, J. G., and Shen, S. S. (2011). Purification and structural analysis of surfactin produced by endophytic bacillus subtilis EBS05 and its antagonistic activity against rhizoctonia cerealis. *Plant Pathology J.* 27 (4), 342–348. doi:10.5423/ppj.2011.27.4.342

Witwicki, M., Lewińska, A., and Ozarowski, A. (2021). *o* -Semiquinone radical anion isolated as an amorphous porous solid. *Phys. Chem. Chem. Phys.* 23 (32), 17408–17419. doi:10.1039/d1cp01596f

Witwicki, M. (2015). Theoretical characterisation of phosphinyl radicals and their magnetic properties: *g* matrix. *ChemPhysChem* 16 (9), 1912–1925. doi:10.1002/cphc.201500121

Witwicki, M., Walencik, P. K., and Jezierska, J. (2020). How accurate is density functional theory in predicting spin density? An insight from the prediction of hyperfine coupling constants. *J. Mol. Model.* 26 (1), 10. doi:10.1007/s00894-019-4268-0

Wu, Y. S., Ngai, S. C., Goh, B. H., Chan, K. G., Lee, L. H., and Chuah, L. H. (2017). Anticancer activities of surfactin potential application of nanotechnology assisted surfactin delivery. *Front. Pharmacol.* 8, 1–22. doi:10.3389/fphar.2017.00761

Yang, S. Z., Wei, D. Z., and Mu, B. Z. (2007). Determination of the structure of the fatty acid chain in a cyclic lipopeptide using GC-MS. *J. Biochem. Biophysical Methods* 70 (3), 519–523. doi:10.1016/j.jbbm.2007.01.005

You, J., Yang, S., and Mu, B. (2015). Structural characterization of lipopeptides from *Enterobacter* sp. strain N18 reveals production of surfactin homologues. *Eur. J. Lipid Sci. Technol.* 117 (6), 890–898. doi:10.1002/ejlt.201400386

Zdziennicka, A., Jańczuk, B., and Wójcik, W. (2003). Wettability of polytetrafluoroethylene by aqueous solutions of two anionic surfactant mixtures. *J. Colloid Interface Sci.* 268 (1), 200–207. doi:10.1016/s0021-9797(03)00702-1

Zhang, J., and Lu, T. (2021). Efficient evaluation of electrostatic potential with computerized optimized code. *Phys. Chem. Chem. Phys.* 23 (36), 20323–20328. doi:10.1039/d1cp02805g

Zhang, Lei, Wang, Z. L., Li, Z.-Q., Zhang, L., Xu, Z. C., Zhao, S., et al. (2010). Wettability of a quartz surface in the presence of four cationic surfactants. *Langmuir* 26 (24), 18834–18840. doi:10.1021/la1036822

Zhao, Y., Yang, S. Z., and Mu, B. Z. (2012). Quantitative analyses of the isoforms of surfactin produced by Bacillus subtilis HSO 121 using GC-MS. *Anal. Sci.* 28 (8), 789–793. doi:10.2116/analsci.28.789

Zou, A., Liu, J., Garamus, V. M., Yang, Y., Willumeit, R., and Mu, B. (2010). Micellization activity of the natural lipopeptide [Glu $_{1}$, Asp $_{5}$] surfactin-C15 in aqueous solution. *J. Phys. Chem. B* 114 (8), 2712–2718. doi:10.1021/jp908675s